UNIVERSIDAD DE SANTIAGO DE CHILE
FACULTAD DE CIENCIAS
Departamento de Física

Quantum correlations and Quantum phase transitions

Natalia Angélica Valderrama Quinteros

Profesor Guía: Juan Carlos Retamal Abarzúa

Tesis para optar al grado académico de Magíster en Ciencia con Mención en Física.

Santiago - Chile
2023

- Acknowledges to Financiamiento Basal para Centros Científicos y Tecnológicos de Excelencia (Grant No. AFB2200001).
- Acknowledges to Vicerrectoría de Posgrado

Abstract

Spin chains or spin networks are a central problem in the study of many-body systems. They are of great interest because they exhibit complex physical phenomena, thanks to the fact that they are strongly correlated systems. Particularly in the zero temperature regime, these systems exhibit quantum phase transitions, which are characterized by distinct changes that arise in the properties of the fundamental state of the system as a non-thermal control parameter is varied. The changes exhibited by a system under a quantum phase transition are usually studied by order parameters characterizing one of the phases in transition, and by looking for discontinuous or singular behavior in the ground state energy of the system. However, it has been some time since it has been known that these changes can also be described through the behavior exhibited by bipartite and multipartite quantum correlations in these systems. These quantum correlations can be studied using correlation estimators, which allow the identification of the states through which the physical system transits when varying the control parameter, on which the Hamiltonian of the system depends. The conceptual framework for these correlation estimators has been incorporated into this type of study thanks to the field of Quantum Information, giving rise to the so-called Quantum Matter field.

In general, approximation methods, both theoretical and numerical, are used to solve these systems, since it is not common to find integrable systems, which have exact solution. Numerical methods include the Density Matrix Renormalization Group (DMRG) algorithm. This method has the advantage of simulating the fundamental state of a finite or infinite chain of spins with satisfactory numerical accuracy, without having to span the entire Hilbert space in the process. This is a very relevant point since this dimension scales exponentially with the number of sites considered in the simulation. In this work, we will study the quantum phase transitions present in the spin-1 Heisenberg XXZ model with single-ion anisotropy. To find the fundamental state of the system, we will use the infinite DMRG algorithm, simulating an infinite chain with open boundary conditions. In particular, we will focus on the bipartite correlations exhibited by the two central sites of the chain. By obtaining the reduced density matrix of these sites we can calculate the quantum correlations they exhibit using Quantum Discord (QD) and Entanglement. By observing the behavior of these correlation estimators, we can determine the quantum phase transitions of the system.

Keywords: Quantum phase transition; Quantum correlation estimator; Quantum Discord; Entanglement; Density Matrix Renormalization Group; Spin chains.

Resumen

Las cadenas o redes de spin constituyen problema central en el estudio de sistemas de muchos cuerpos. Son de gran interés pues exhiben fenómenos físicos complejos, gracias a que son sistemas fuertemente correlacionados. En particular en el régimen de temperatura cero estos sistemas exhiben transiciones de fase cuánticas, las cuales se caracterizan por exhibir cambios distintivos que surgen en las propiedades del estado fundamental del sistema a medida que un parámetro de control no térmico es variado. Los cambios que exhibe un modelo bajo una transición de fase cuántica se suele estudiar mediante parámetros de órden que caractericen a una de las fases, y mediante comportamientos discontinuos o singulares en la energía del estado fundamental del sistema. Sin embargo, ha pasado tiempo desde que se sabe que estos cambios también pueden ser descritos a través del comportamiento que exhiben las correlaciones cuánticas bipartitas y multipartitas en estos sistemas. Estas correlaciones cuánticas pueden estudiarse usando estimadores de correlación, los cuales permiten identificar los estados por los cuales transita el sistema físico al variar el parámetro de control, del cual depende el Hamiltoniano del sistema. El marco conceptual para estos estimadores de correlaciones cuánticas se ha incorporado a este tipo de estudios gracias al campo de la Información Cuántica, dando lugar al denominado campo de estudio de la Materia Cuántica.
En general para resolver estos sistemas se suelen usar métodos de aproximación, tanto de cálculo como numérico, pues no es lo común encontrarse con sistemas integrables que poseen solución analítica. En el ámbito de los métodos numéricos se encuentra el algoritmo de Density Matrix Renormalization Group (DMRG). Este método posee la ventaja de simular el estado fundamental de una cadena finita o infinita de spines con buena precisión numérica, sin tener que recorrer todo el espacio de Hilbert en el proceso. Este es un punto muy relevante, ya que esta dimensión escala exponencialmente con el número de sitios que se consideran en la simulación.
En este trabajo estudiaremos las transiciones de fase cuánticas presentes en el modelo de Heisenberg XXZ de spin 1 con anisotropía de ión. Para encontrar el estado fundamental del sistema, utilizaremos el algoritmo de DMRG infinito, simulando una cadena infinita con condiciones de borde abiertas. En particular nos centraremos en las correlaciones bipartitas que exhiban los dos sitios centrales de la cadena. Obteniendo la matriz densidad reducida de estos sitios podemos calcular las correlaciones cuánticas que presentan mediante los estimadores de correlación Quantum

Discord (QD) y Entrelazamiento. Al observar el comportamiento de estas funciones, podremos determinar las transiciones de fase cuánticas del sistema.

Palabras claves: Transición de fase cuántica; Estimador de correlación cuántica; Quantum Discord; Entrelazamiento; Density Matrix Renormalization Group; Cadenas de spin.

Dedicatory

Frase 1

Autor 1.

Frase 2

Autor 2.

Agradecimientos

Son muchas las personas a quienes deseo agradecer, puesto que han contribuido de diferentes maneras a mi vida académica y privada. Quisiera comenzar por agradecer a mi profesor guía, el Dr. Juan Carlos Retamal por toda la formación que me ha entregado durante mi carrera de pregrado y postgrado. No sólo me ha entregado herramientas académicas para enfrentarme a la investigación, sino que también me ha mostrado contención y amabilidad en los momentos donde la carga de este trabajo me hizo sentir abrumada. Extiendo este agradecimiento al Dr. Guillermo Romero, quien también ha formado parte importante en mi formación como investigadora, quien me enseñó (por repetición) que pedir ayuda ante problemas que nacen del proceso natural de investigar está bien, pues la ciencia se hace en comunidad. Agradezco también a Francisco Albarrán por su siempre buena disposición y ánimo para resolver dudas. Manifiesto mi gratitud también a los profesores y profesoras que han sido parte de mi formación académica universitaria, especialmente a quienes forman parte del programa de postgrado. Gracias por siempre escuchar y responder mis infinitas preguntas en clases.

Deseo agradecer a mi familia, por todo el amor que me han entregado. A mis padres, quienes, a pesar de venir de un lugar humilde, siempre incentivaron mi curiosidad ante el mundo y lograron darme herramientas para llegar hasta acá. A mis hermanos, quienes afrontaron las adversidades de la vida y lograron darles vuelta, propiciando una situación más favorable para mí. A ustedes, gracias por siempre apoyarme.

Quisiera agradecer a mis amigos, por siempre confiar en mí y escucharme cuando lo necesité. Me doy cuenta a medida que crezco, que la amistad se vuelve algo difícil de mantener ante las responsabilidades de la vida. Espero contar con su amistad y apoyo en las siguientes instancias donde deba escribir nuevos agradecimientos.

Agradezco profundamente a mi pareja, Luciano. Contar con tu apoyo y confianza en mí me inspira profundo valor ante mis objetivos.

Finalmente agradezco a la Vicerrectoría de Postgrado y al centro CEDENNA. Este trabajo de tesis fue financiado con el Financiamiento Basal para Centros Científicos y Tecnológicos de Excelencia (Grant No. AFB2200001).

Acknowledgements

Thanks to Vicerrectoría de Postgrado and the CEDENNA center. This thesis work was funded by the Financiamiento Basal para Centros Científicos y Tecnológicos de Excelencia (Grant No. AFB2200001).

Notations

In this thesis, we set $\hbar = 1$.

Contents

List of Tables

List of Figures

Chapter 1

Introduction

Spin chains are many-body systems that exhibit several exciting phenomena to study, such as quantum phase transitions (QPT), which are phase transitions driven by quantum fluctuations at cero temperature, when a parameter of the Hamiltonian is varied (magnetic field, anisotropy, etc.). Traditionally the QPTs are detected by discontinuous changes in the ground state energy or in the behavior of observables associated with the system [1]. However, it has been a while since the knowledge of the link between QPT and quantum correlations, and how by means of Quantum information theory this link has been exploited very successfully. The behavior of several well-known systems has been studied, particularly in spin $\frac{1}{2}$ systems. In higher dimensions, however, the work is not as extensive. This is despite higher dimensional systems showing remarkable richness and complexity in their phase diagrams. In spin-1 systems the behavior that some systems should have is known. Still, the findings of this have been reported by approximation methods or numerical methods in general, since for higher spin systems an analytical result is not usually available.

It is in this place where is framed this thesis. We want to study the spin-1 Heisenberg XXZ model with single-ion anisotropy and the QPTs that this model exhibits. To accomplish that objective, we have covered and connected different areas. One of these has been quantum correlation estimators, elements borrowed from the Quantum Information domain, such as Entanglement and Quantum Discord (QD). These correlation estimators require knowledge of the state of the system in question, which connects us with the numerical aspect of this thesis, the Density Matrix Renormalization Group (DMRG) algorithm. To study the quantum correlations, we need to simulate the ground state of the system, which is made under the technique of DMRG, a numerical technique that has proven to be very useful and accurate in simulating strongly correlated systems such as spin chains. As our work centralizes on studying bipartite correlations, we pay particular attention to the central sites of the simulated chain, to whose reduced density matrix we will apply these correlation measures. The latter requires an optimization process since some correlation estimators are defined on the basis of a convex roof problem. After verifying if the optimization process is

correct, the quantum correlations of the system are calculated, where the QPTs will be finally located. As can be seen, this thesis covers a non-trivial topic through the use of interdisciplinary tools and knowledge.

The outline of this thesis is the following. In the first section of this introduction, the background of the problem and the state of the art are presented. The second chapter provides the theoretical and conceptual bases from Quantum information theory necessary to understand this thesis. The third chapter introduces the DMRG algorithm in its infinite and finite variations and the considerations for its correct application and use. The fourth chapter introduces formally the concepts of QPT and some distinguished spin-1/2 models with the corresponding QPTs. Chapter five presents the results, which are divided into two sections. The first has to do with results that test the performance of our optimization algorithm to demonstrate the reliability of the results obtained with it, in terms of quantum correlations. And in the second section, those results have to do with detecting QPTs of the known spin-1/2 models, to ensure the correct performance of our DMRG algorithm, and the study of quantum correlations in the spin-1 XXZ Heisenberg model with single-ion anisotropy.

1.1 Background and state of art

The phases of matter have been the object of fascination since old times, just by observing everyday life very natural questions arise, such as why some things are liquid and others solid or gaseous. Why do the states of matter change with temperature? The central concept behind this phenomenology is related to phase transitions. A phase of matter can be distinguished because, in general, it has a macroscopic order that defines it, which changes as some thermodynamic parameter is varied, for example, the temperature. An everyday example of this is the change that water undergoes during the boiling process. Another, perhaps familiar to those involved in magnetism, is the transition from a ferromagnetic to a paramagnetic material, where magnetization disappears after the phase transition when the critical temperature is reached and exceeded.

Traditionally, the study of phase transitions is carried out by analyzing the free energy of the system, and correlation functions between different observables and their respective correlation length, such as spin-spin correlations [2]. It is also known that when a system is close to certain phase transitions it presents a scaling phenomenon [3–6], which basically shows how the behavior of a finite system gives special signals around a particular point, such that if the thermodynamic limit is taken this point is the critical point where occurs a phase transition. The previously mentioned examples correspond to the so-called classical phase transitions, where thermal fluctuations are the ones that play the relevant role in producing a change of state of a system. This thesis work is framed in studying quantum phase transitions, which occur at temperature $T = 0$ [1, 2]. This implies that thermal fluctuations are not responsible for the transition. When we move to the

quantum regime, quantum fluctuations are the ones that determine that a system changes from one phase to another, when a control parameter is modulated, which can be the external magnetic field, a coupling constant, etc. As strange as it may seem at first, the way to study this type of phase transition at temperature $T = 0$ does not vary with respect to the traditional approach. One can still study the energy, critical exponents, and correlation lengths, which has been one way of describing quantum phase transitions. However, a new way to study these phase transitions came from the work of Osterloh, Amico, Falci, and Fazio [7] who incorporated elements from the field of Quantum Information, such as quantum Entanglement, to approach the description of phase transitions.

What was revolutionary about this paper was that they studied the phase transition of a system well known to the condensed matter area, but emphasized the scaling of bipartite Entanglement to nearest and next-nearest neighbors in the chain. The considered system was the spin $\frac{1}{2}$ ferromagnetic chain with an exchange coupling J in a transverse magnetic field of strength h,

$$H = \Big(\sum_{i}^{N} -J\big(\frac{(1+\gamma)}{2}\sigma_i^x\sigma_{i+1}^x - \sum_{i}^{N}\frac{(1-\gamma)}{2}\sigma_i^y\sigma_{i+1}^y\big) - h\sigma_i^z \Big) \tag{1.1.1}$$

where σ^α are the Pauli matrices $\{\alpha = x, y, z\}$ and N is the number of sites in the chain. This model is equal to the Ising model when $\gamma = 1$, and to the XY model when $\gamma = 0$.

For the first time, a concept of Quantum Information associated with correlations without classical counterparts was used to show that phase transitions could be detected by changes in the quantum correlations of a system. In the paper, they focus on the bipartite Entanglement of 2 spins, at the i and j positions. The relevant physical information of the problem was derived from the density matrix of the system, obtained from the ground state. Only the pair of sites of interest were considered and the rest was traced out from the total density matrix, leaving the reduced density matrix of sites i and j, $\rho_{i,j}$. This matrix represents the bipartite mixed state of two spins. By the late '90s, a method to quantify Entanglement in systems like this was already known thanks to Wootters [8] and his analytical formula for calculating Concurrence, and the relation of Concurrence to Entanglement of formation.

In the paper, they were able to write the density matrix by taking advantage of the symmetries of the system and also managed to fix the structure of ρ in a form that allowed them to write the non-zero elements of the matrix based on different correlation functions. With this, they were able to evaluate the Concurrence exactly as a function of the relative position $|i - j|$ between the spins and as a function of the distance $|\lambda - \lambda_c|$ from the critical point, where $\lambda = \frac{J}{2h}$.

The results for the Ising case were captured in figure 1.1. The change in the ground state was studied considering the first derivative of the Concurrence of the nearest neighbor with respect to the reduced coupling strength λ. The different curves correspond to different lattice sizes, and

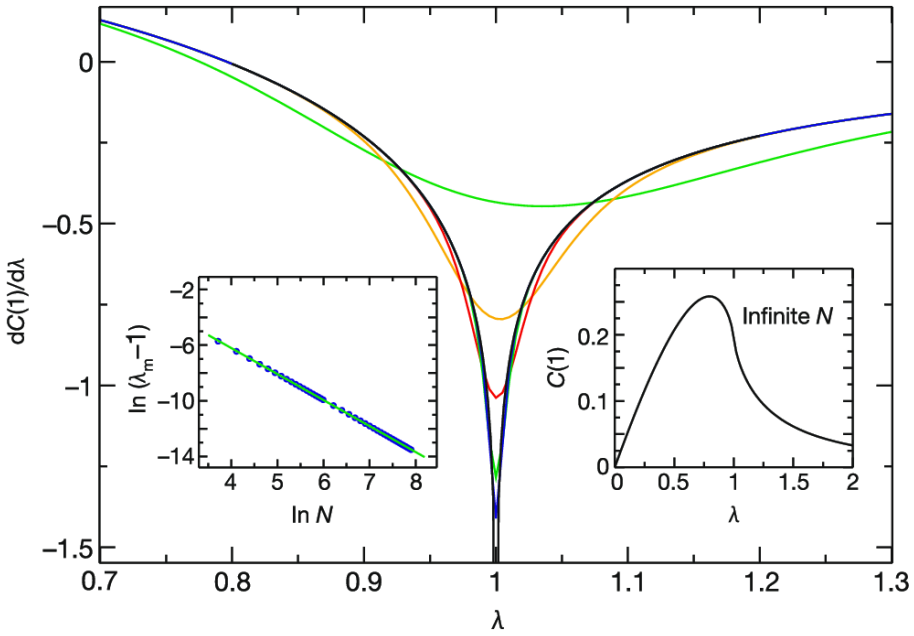

Figure 1.1: The first derivative of the nearest neighbor Concurrence with respect to the reduced coupling term λ is studied for different lattice sizes. The minimum becomes more pronounced as the system size is increased. The left inset shows how the minimum position change and tends as $N^{-1.87}$ towards the critical point $\lambda_c = 1$. The right inset shows the Concurrence $C(1)$ itself for an infinite system [7].

the black one shows the behavior in the thermodynamic limit, where $\partial_\lambda C(1)$ diverges while it approaches the critical value as

$$\frac{dC(1)}{d\lambda} = \frac{8}{3\pi^2} \ln|\lambda - \lambda_c| + const. \tag{1.1.2}$$

From the finite size scaling study, the position of the minimum λ_m scales as $\lambda_m \sim \lambda_c + N^{-1.87}$, and its value diverges logarithmically with increasing the system size as

$$\left.\frac{dC(1)}{d\lambda}\right|_{\lambda_m} = -0.2702 \ln N + const. \tag{1.1.3}$$

According to the scaling ansatz, taking the ratio between the two prefactors of the logarithm gives the exponent that governs the divergence of correlation length ν. For the case of the Ising model, $\nu = 1$ and this is consistent with $8/3\pi^2 \approx 0.2702$. All of the above analysis was also performed for the next nearest neighbors, but in that case, taking the second derivative of the Concurrence. The results agreed on the same value of the critical exponent of the Ising model.

Another relevant conclusion obtained from this paper was that universality in Entanglement was proved, i.e., that the critical properties of Entanglement depend only on the dimensionality of the system and the broken symmetry in the ordered phase. This was proved in a robust and general way for $\gamma \neq 1$.

Another work related to Entanglement in spin chains for phase transitions is that of Osborne and Nielsen [9]. This paper, published shortly after, also demonstrates the connection between Entanglement and quantum phase transitions in the XY model and the Ising model.

Many papers embarked to use this existing relationship by borrowing concepts from Quantum Information to study QPTs, obtaining successful results [10–20], between the correlator estimators used in these articles are Entanglement [12, 14–16, 20], Quantum Fidelity [11, 19], Quantum Discord [13, 15–17] and Quantum Coherence [17, 21], among others, just to mention a few.

Particularly relevant for this thesis are the references [12, 17]. In the first article, the spin-1 XXZ Heisenberg model with a single ion anisotropy is examined, obtaining a phase diagram of the model using negativity. In the second, the QPTs of the spin 1 XXZ Heisenberg model are studied using Quantum Discord. .

With all the above context given, it is clear why it is of interest to carry out this thesis.

Chapter 2

Quantum information elements

2.1 Summary

In this chapter, we introduce some fundamental concepts in quantum information that we will use during the development of this thesis. First, we introduce the representation of a quantum state in quantum mechanics for the case of isolated systems and systems interacting with an environment. In addition, we introduce the notion of quantum correlations embedded in a quantum state, and the quantum correlations estimators, such as Entanglement and QD. Finally, the optimization algorithm used in the computation of quantum correlations will be described.

2.2 Fundamentals

2.2.1 Pure state

A fundamental postulate of quantum mechanics states that every isolated quantum system is described by a state vector $|\Psi\rangle$ that belongs to a Hilbert space $\mathcal{H}$ [22]. A Hilbert space is a linear vector space on complex numbers with an inner product. The state vector satisfies the condition of being normalized according to the statistical interpretation of the wave function given by the Born postulate, i.e, the norm is equal to 1,

$$\langle\Psi|\Psi\rangle = 1 \tag{2.2.1}$$

The vector state can be spanned by a set of orthonormal eigenvectors $\{|\phi\rangle\}$ of an observable $\hat{O}$,

$$|\Psi\rangle = \sum_i c_i \, |\phi_i\rangle \tag{2.2.2}$$

where the coefficients $\{c_i\}$ are the probability amplitudes. In this form, the normalization condition in 2.2.1 is equivalent to

$$\sum_i |c_i|^2 = 1$$

This kind of state embodies all information needed to characterize a system, that is, it can be known all the relative phases between the eigenstates into which the vector state is spanned.
The measurement for pure states is carried out by means of projective measurement, which consist of a set of observables $\{\hat{O}_\omega\}$ acting in the space of the system to be measured. The observables have spectral decomposition

$$\begin{aligned} \hat{O} &= \sum_\omega \omega \left|\phi_\omega\right\rangle \left\langle\phi_\omega\right| \\ &= \sum_\omega \omega P_\omega \end{aligned} \tag{2.2.3}$$

where $P_m = \left|\phi_\omega\right\rangle \left\langle\phi_\omega\right|$ are the projectors onto the eigenspace of $\hat{O}$ with eigenvalue ω. The projectors fulfill two conditions, the first one is the completeness relation and the second one is the relation of orthogonality. Both conditions can be represented as

$$\sum_\omega P_\omega^\dagger P_\omega = \mathrm{I} \tag{2.2.4}$$

$$P_{\omega'} P_\omega = \delta_{\omega'\omega} P_\omega \tag{2.2.5}$$

For the expectation value, we can derive it from equation 2.2.3 projecting the operator into the state $|\Psi\rangle$

$$\left\langle\Psi\right| \hat{O} \left|\Psi\right\rangle = \sum_\omega p(\omega)\, \omega \tag{2.2.6}$$

where the probability of obtaining a certain eigenvalue ω from $\hat{O}$ is

$$p(\omega) = \left\langle\Psi\right| \hat{P}_\omega \left|\Psi\right\rangle \tag{2.2.7}$$

and the state $|\Psi\rangle$ after the measure becomes

$$\frac{\hat{P}_\omega \left|\Psi\right\rangle}{\sqrt{p(\omega)}} \tag{2.2.8}$$

Since the completeness equation 2.2.4 is satisfied, the probability $p(\omega)$ adds up to 1.
The evolution of an isolated system $|\Psi\rangle$ is determined by the Schrödinger equation,

$$i\hbar\frac{\mathrm{d}\,|\Psi\rangle}{\mathrm{d}t} = \hat{H}\,|\Psi\rangle \tag{2.2.9}$$

which is equivalent to saying that the vector state evolution is described for a unitary transformation U.
These postulates of quantum mechanics are useful to characterize a collection of identical systems, described by the same state vector. Nevertheless, when we are faced with describing a group of non-identical systems, we must take another path to represent a mixture of systems. The mathematical language we seek is that of the density matrix. This formalism is particularly useful when describing composite systems or a mixed state, as we shall see below.
For a pure state $|\Psi\rangle$, the associated density matrix is defined as the outer product of the state with itself.

$$\rho = |\Psi\rangle\,\langle\Psi| \tag{2.2.10}$$

If we want to translate the concept of measure for some observable $\hat{O}$, it can be done from the equation 2.2.6, obtaining

$$\langle\hat{O}\rangle = Tr\left(\rho\,\hat{O}\right) \tag{2.2.11}$$

And in terms of the evolution of this system, we can use the fact that the evolution of an isolated system is determined by a unitary transformation U, and we can write it as

$$\rho \xrightarrow{U} U\,\rho\,U^{\dagger} \tag{2.2.12}$$

In the following sections, we will discuss the properties that ρ must fulfill in order to be a density matrix representing the quantum state of a system.

2.2.2 Composite system and density matrix

It is of interest to introduce fundamental concepts for many-body systems since one of the essential objectives of this thesis is to study spin chains. We have previously introduced the notion of pure states, which represent a whole isolated system, independent of the number of constituents of the total system. When we have a system composed of two or more parties, the Hilbert space of the overall system is the tensor product of the individual Hilbert spaces for each component, that is, $\mathcal{H}_{\mathcal{T}} = \mathcal{H}_1 \otimes \mathcal{H}_2 \otimes ... \otimes \mathcal{H}_N$ [22]. Assuming each part of the total state system having the same dimension d, then, the physical dimension of the composite system is d^N.
However, it is not always necessary or required to study all the parts of a system. Often it is only of interest to take a bipartite system, as the two central sites of a spin chain, in order to obtain the

desired information, as Entanglement, for example. Taking an infinite spin chain as an illustration, we can divide this system into the part of interest denoted $\mathcal{S}$ and the rest of the system is denoted $\mathcal{E}$ as the environment. To be interested only in the information related to the system $\mathcal{S}$ involves discarding the information of the environment, this implies that the *reduced* system now can not be described for a state vector.

As we saw in the latter subsection, a pure state can be represented as a density matrix. Let us suppose a global state that represents the pure state of a composite system $\mathcal{T}$, the general form to write this state as a density matrix is

$$\rho_{\mathcal{T}} = |\psi\rangle \langle\psi| \tag{2.2.13}$$

where $|\psi\rangle \in \mathcal{H}_{\mathcal{T}}$, and the total Hilbert space $\mathcal{H}_{\mathcal{T}}$ is the composition of each particular Hilbert space of the constituents. Let us consider now we only wants to access the information about the subsystem $\mathcal{S}$. Suppose we measure an observable $\hat{O}_S$ defined locally on the system $\mathcal{S}$, which implies applying the identity matrix to the other parts corresponding to $\mathcal{E}$. We already know from the equation 2.2.6 that the expectation value of this observable can be written as

$$\langle \hat{O}_S \rangle = tr\left(\rho_{\mathcal{T}} \hat{O}_{\mathcal{S}}\right) \tag{2.2.14}$$

where the trace is over $\mathcal{S}$ and $\mathcal{E}$ states. Let us denote by $\rho_{(\mathcal{S}+\mathcal{E})}$ density matrix of the total system involving degrees of freedom related to $\mathcal{E}$ and $\mathcal{S}$. In terms of this, we can write

$$\begin{aligned} \langle \hat{O}_S \rangle &= tr_{(\mathcal{S}+\mathcal{E})}\left(\rho_{(\mathcal{S}+\mathcal{E})} \hat{O}_{\mathcal{S}}\right) \\ &= \sum_{\mathcal{S}} \sum_{\mathcal{E}} \langle\psi_{\mathcal{S}}| \langle\psi_{\mathcal{E}}| \rho_{(\mathcal{S}+\mathcal{E})} \hat{O}_{\mathcal{S}} |\psi_{\mathcal{S}}\rangle |\psi_{\mathcal{E}}\rangle \\ &= \sum_{\mathcal{S}} \langle\psi_{\mathcal{S}}| \left(\sum_{\mathcal{E}} \langle\psi_{\mathcal{E}}| \rho_{(\mathcal{S}+\mathcal{E})} |\psi_{\mathcal{E}}\rangle \right) \hat{O}_{\mathcal{S}} |\psi_{\mathcal{S}}\rangle \end{aligned} \tag{2.2.15}$$

By dividing the degrees of freedom in this way, the trace in the pure states defining the $\mathcal{E}$ part has no effect on the operator defined locally in $\mathcal{S}$, so we can define the reduced state for $\mathcal{S}$ as the total state $\mathcal{T}$ being traced out from the degrees of freedom of the environment $\mathcal{E}$. This is known as the reduced density matrix,

$$\rho_{\mathcal{S}} = \sum_{\mathcal{E}} \langle\psi_{\mathcal{E}}| \rho_{(\mathcal{S}+\mathcal{E})} |\psi_{\mathcal{E}}\rangle \tag{2.2.16}$$

with this let us note that the information we are interested in from the subset of the total system depends only on the system variables $\mathcal{S}$. To the operation of tracing a portion of the degrees of freedom of an entire group, it is called partial trace. The equation 2.2.15 results in

$$\langle \hat{O}_S \rangle = \sum_{\mathcal{S}} \langle\psi_{\mathcal{S}}| \rho_{\mathcal{S}} \hat{O}_{\mathcal{S}} |\psi_{\mathcal{S}}\rangle \tag{2.2.17}$$

2.2.3 Mixed state

In general, when we have a composite system where we focus only on a subset of the global system, the quantum state characterizing the state of the subset is no longer a pure state. This state is obtained partially by tracing degrees of freedom that we do not observe and consequently, we neglect information about them. This loss of information means that the state describing the subset can be represented by an incoherent superposition of different pure states. These pure states are not necessarily eigenstates of the same observable, i.e, orthogonal to each other. A mixed state is usually called a statistical ensemble, because of the introduction of the classical probability p_i that weights the different mixture of pure states $|\psi_i\rangle$. To illustrate the latter, think of a beam of electrons whose spin direction is not determined, say 70% are in the S_x direction and 30% are in the S_z direction [23]. This example represents a mixture of the collection of individual parts where it is impossible to describe the total system under the same pure state.

The formalism of the density matrix is introduced to treat mixed states. In general, a quantum state represented by a density matrix is not necessarily pure, as we have mentioned before. Generalizing the density matrix for a pure state defined in equation 2.2.10, for an ensemble as $\{p_i, |\psi_i\rangle\}$, we define

$$\rho = \sum_j p_j \, |\psi_j\rangle \, \langle\psi_j| \tag{2.2.18}$$

as the density matrix for a mixed state, where $\sum_j p_j = 1$. The ensemble defining a mixed state is not unique.

It is worth mentioning that when measuring an observable in a mixed state, one is calculating an average of the possible average values $\hat{O}_i = \langle\psi_i| \hat{O} |\psi_i\rangle$ of the observable $\hat{O}$ on each pure state in the decomposition, given by 2.2.11, that is

$$\begin{aligned} \langle\hat{O}\rangle_{stat} &= \sum_i p_i \hat{O}_i \\ &= Tr\left(\rho\hat{O}\right) \end{aligned} \tag{2.2.19}$$

It can be shown that density matrix ρ must fulfill the following requirements

1. $\rho = \rho^\dagger$
2. $Tr(\rho) = \sum_j p_j = 1$
3. $\rho \geq 0$
4. $Tr\rho^2 \leq 1$

The first one indicates that the density matrix must be Hermitian. The second reflects the statistical nature of the density matrix. The third property establishes that the density matrix must be semi-

positive, that is, it can only have non-negative eigenvalues. This implies that we can always find a spectral decomposition of ρ given by $\rho = \sum_k \alpha_k |\phi_k\rangle \langle\phi_k|$, where α_k are the eigenvalues and $|\phi_k\rangle$ the eigenvectors. Finally, the last property indicates that the non-diagonal elements are limited by this constraint, in which the equality is satisfied for a pure state.

2.3 Correlation estimators

Statistically, correlation is a measure of the order in a system, quantifying the association between the fluctuation of 2 variables with respect to the other. This order is an average measure of two physical quantities, in space and time, that describes the strength of this relationship by means of a mathematical function called correlation function. Throughout this thesis, we will not refer to quantum correlations in this traditional sense, but rather when we refer to quantum correlations we will be talking about relationships that do not necessarily have a classical counterpart nor can they be quantified by a correlation function as described above. Quantum correlations may arise as a consequence of quantum nature as such, as Entanglement, just as from the competition between the different interactions that dominate the system in different regimes of a driving parameter. In the following will be introduced the correlation estimators that quantify the two main types of quantum correlations used in this work, Entanglement, and QD.

2.3.1 Entanglement measures

Entanglement is a quantum correlation without any equivalent in its classical counterpart. It is a direct consequence of the superposition principle, which arise from the property of linearity of the Hilbert space, i.e, if a system can be in a normalized vector state $|\phi_1\rangle$ or $|\phi_2\rangle$, also can be in a linear combination of both $\alpha |\phi_1\rangle + \beta |\phi_2\rangle$ - with α and β satisfying the standard normalization condition $|\alpha|^2 + |\beta|^2 = 1$ -. This was the cause of a well-known scientific dispute, the EPR paradox in 1935 [24], where the plausibility of this property was discussed. It was not until the '70s when this fundamental concept was experimentally proven correct by a generalization of Bell's inequalities [25, 26], and even later in the '90s when becomes relevant due to quantum teleportation [27] and quantum computation with the Shor algorithm [28].
To measure Entanglement there are several correlation estimators, among which the Entanglement of formation (Eof) stands out.

Entanglement of Formation

For a pure bipartite state $|\psi_{AB}\rangle$, the Von Neumann entropy is used as a measure of Entanglement.

$$E_f(|\psi_{AB}\rangle) = S(\rho_j) = -tr\left(\rho_j log\left(\rho_j\right)\right) \tag{2.3.1}$$

where ρ_j is the reduced density matrix of one of the parties of the total system. The index $j = A, B$ indicates that the Von Neumann entropy can be calculated with any of both density matrices of the reduced system.

For a mixed state, the Eof is defined as the minimum Entanglement generated by the ensemble $\{p_i, |\psi_i\rangle\}$

$$E_f(\rho_{AB}) = min \sum p_i E_f(|\psi_i\rangle) \tag{2.3.2}$$

where $E_f(|\psi_i\rangle)$ is defined by equation 2.3.1. To find the minimum of equation 2.3.2, we must perform this calculation on different ensembles describing the same mixed state. This is achieved by performing a purification process on the system. This purification process implies a problem of optimization, for which the details will be aborded in the section of the same name below. The optimization problem of Eof is not an easy task from the point of view of computational resources. This highlights the importance of having analytical expressions. In this line, it is known in the literature that closely related to Eof is concurrence.

Concurrence

Wootters developed a way to quantify Entanglement in an analytic manner for qubit systems [8], for both pure and mixed states. For pure states, one can write the concurrence $\mathcal{C}$ as

$$\mathcal{C} = 2|\langle\psi^*|\sigma_y \otimes \sigma_y |\psi\rangle| \tag{2.3.3}$$

where $|\psi^*\rangle$ is the conjugate state of $|\psi\rangle$, and σ_y is the second Pauli matrix.

On the other hand, for a mixed state, one can write the concurrence as

$$\mathcal{C} = max\left(0, \sqrt{\lambda_4} - \sqrt{\lambda_3} - \sqrt{\lambda_2} - \sqrt{\lambda_1}\right) \tag{2.3.4}$$

where λ_i are the eigenvalues of the matrix $\rho\,(\sigma_y \otimes \sigma_y)\rho^*(\sigma_y \otimes \sigma_y)$ in decreacing order. It should be noted that this way of calculating concurrency requires the density matrix to have at least two eigenvalues different from 0.

Both, for the mixed case and the pure case, the relationship between concurrency and the Eof is given by replacing in the following expression the corresponding equation for concurrence

$$E(x) = x\, log_2\, x - (1-x) log_2(1-x) \tag{2.3.5}$$

$$x = \frac{1}{2}(1 + \sqrt{1 - \mathcal{C}^2}) \tag{2.3.6}$$

Unfortunately, there is no analytical result to calculate a figure of merit such as concurrency or Entanglement in higher dimensions.

Negativity

Since calculating Eof is an arduous task, other measures serve as upper/lower bounds for Entanglement. Negativity is a lower bound of Entanglement [29] and is related to Peres' criterion of separability [30]. In his work, Peres noted that if a bipartite separable state ρ_{AB} is partially transposed -partially in the same sense as *partially* tracing-, then the partially transposed matrix $\rho^{T_{A/B}}$ remains a physical state. In the same year it was shown [31] that this separability criterion is sufficient only for low dimensions, such that the total dimension of the bipartite system is $d_{AB} \leq 6$, i.e., $2 \otimes 2$ or $3 \otimes 2$ systems. This is how the violation of this criterion allows the detection of Entanglement. In the case of Negativity, it is related to the degree to which $\rho^{T_{A/B}}$ fails to be positive [29]. Negativity is defined as

$$\mathcal{N} = \frac{||\rho^{T_B}||_1 - 1}{2} \tag{2.3.7}$$

where the operation T_B is the partial transposition of the party B of the total global density matrix ρ. The operation $||(...)||_1$ means the sum of all negative eigenvalues of the partial transpose matrix. In general, this quantity is notably easier to calculate than Eof, especially when working with higher spins.

2.3.2 Quantum Discord

Although Entanglement was long thought to be the only type of quantum correlation existing in a bipartite system, this was discarded due to the work of Olivier and Zurek [32], and independently of Henderson and Vedral [33]. The work of these researchers focused on finding a quantum analog of Mutual Information (MI), a concept of classical information theory. It was known that mutual information can be measured by two equivalent expressions at the classical level,

$$\begin{aligned} \mathcal{I}(A:B) &= H(A) + H(B) - H(A,B) \\ \mathcal{J}(A:B) &= H(A) - H(A/B) \end{aligned} \tag{2.3.8}$$

$\mathcal{I}(A:B)$ is the MI, which embodies all correlations of a system, and $\mathcal{J}(A:B)$ is the locally accessible MI, as the latter depends on the local measurement of a part of the system. $H(.)$ is the Shannon entropy, $H(A,B)$ is the joint entropy and $H(A|B)$ is the conditional entropy. The quantum analog of this classical entropy was materialized in the Von Neumann entropy $S(\rho)$. However, in order to take the conditional Shanon entropy into a quantum version, it was necessary to introduce the concept of conditionality in a quantum way. In this sense, the quantum version of equation

2.3.8 is

$$\mathcal{I}(\rho_{AB}) = S(\rho_A) + S(\rho_B) - S(\rho_{AB}) \tag{2.3.9}$$

$$\mathcal{J}(\rho_{AB}) = S(\rho_A) - S(\rho_{A|B}) \tag{2.3.10}$$

here $\mathcal{S}(\rho_{A|B})$ is the entropy of the reduced state of A after a projective measurement has been performed on subsystem B. The projective measures are carried out by a set of operators Π_k^B acting only on subsystem B. The explicit form of writing the projected state is

$$\rho_{A|B}^k = \frac{1}{p_k} \left(\mathrm{I} \otimes \Pi_k^B\right) \rho_{AB} \left(\mathrm{I} \otimes \Pi_k^B\right) \tag{2.3.11}$$

where $p_k = Tr(\mathrm{I} \otimes \Pi_k^B \, \rho_{AB} \, \mathrm{I} \otimes \Pi_k^B)$ is the probability of obtaining the outcome k. The conditional entropy is

$$S(\rho_{A|B}) = \sum_k p_k S(\rho_{A|\{\Pi_k^B\}}) \tag{2.3.12}$$

With the introduction of the measurement dependence to the equation 2.3.10, we have a quantity at which we can maximize the classical correlations by choosing a basis that achieves this result; while in the equation 2.3.9 we have all the classical and quantum correlations present in the system. By taking the difference between these, we obtain a measure that exclusively encompasses correlations of purely quantum origin, this is known as Quantum Discord (QD)

$$\begin{aligned} \mathcal{D} &= \mathcal{I} - \max_{\{\Pi_k\}} \mathcal{J} \\ &= S(\rho_B) - S(\rho_{AB}) + \min_{\{\Pi_k\}} S(\rho_{A|k}) \end{aligned} \tag{2.3.13}$$

QD has been demonstrated to be a useful tool in the study of correlations, not only in QPT but also in thermal correlations [15, 16, 21] and therefore has been considered as a resource for quantum computation when there is no Entanglement [34].

2.4 Optimization algorithm

In order to calculate Eof from equation 2.3.2, as well as to calculate QD in equation 2.3.13, it is necessary to solve a convex roof problem. Based on the work in [35], we describe a numerical method to solve this problem, which foundation is decomposing a unitary matrix.

For the first case of Eof, it is necessary to sample the possible pure-state decompositions of ρ. This is carried out by a process called purification, which uses the idea that any mixed state can be taken as a reduced system of a larger pure state. Denoting $|e_i\rangle$ the orthonormal set of vectors of

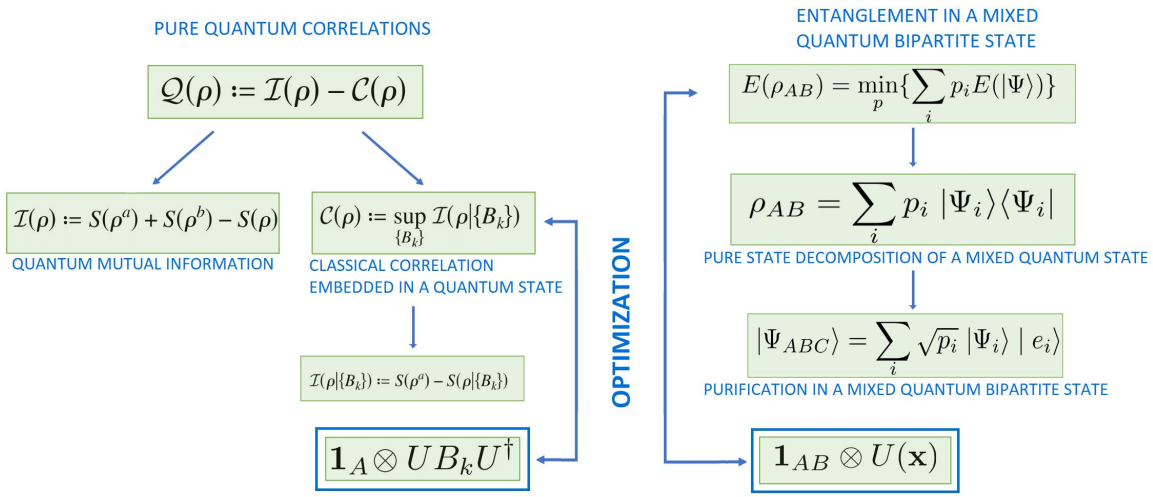

Figure 2.1: Summary diagram for optimization problem in quantum correlations. On the left in panel a) the Quantum Discord calculation is shown, while in panel b) we have the process of purification of a quantum state.

the environment, we can write the purification of the state in equation 2.2.18 as

$$|\Phi\rangle = \sum_{i=1}^{N} \sqrt{p_i} \, |\psi_i\rangle \, |e_i\rangle \tag{2.4.1}$$

N is the number of pure states in equation 2.2.18. The dimension of the vector space of the environment is not constrained to N since we can consider infinite contributions of $p_{i>N} = 0$, so we can vary arbitrarily the dimension of the purification space. The way of searching for different purifications that result in the same reduced state ρ is achieved by rotating the subspace elements of the environment through a unitary transformation,

$$U = \mathrm{I} \otimes U_e \tag{2.4.2}$$

and then tracing out the environment's elements.

In the case of the calculation of QD, the same idea can be achieved. To find all possible projective measures Π_i we can perform unitary rotations in the subspace of B, obtaining new projective measurements as follows

$$\widetilde{\Pi}_i^B = U_B \Pi_i^B U_B^\dagger \tag{2.4.3}$$

Understanding that both problems can be solved by generating this unitary matrix, now we have to build it. It is known that a unitary matrix of dimension $M \times M$ can be decomposed into the

product of $\frac{M(M-1)}{2}$ unitary operations [22]

$$U_{k,n} = \begin{bmatrix} 1 & 0 & .. & & & & & & & \\ 0 & 1 & & & & & & & & \\ : & & \ddots & & & & & & & \\ & & & u_{k,n} & & & u_{k,k+n} & & & \\ & & & & \ddots & & & & & \\ & & & & & \ddots & & & & \\ & & & u_{k+n,n} & & & u_{k+n,k+n} & & & \\ & & & & & & & \ddots & & : \\ & & & & & & & & 1 & 0 \\ & & & & & & & .. & 0 & 1 \end{bmatrix} \tag{2.4.4}$$

where $k = 1, 2, \cdots, M-1$ and $n = 1, 2, \cdots, M-k$. Each unitary matrix $U_{k,n}$ can be parametrized in terms of three arbitrary parameters, such that

$$\begin{aligned} u_{k,k} &= A \\ u_{k+n,k} &= B \\ u_{k,k+n} &= B^* \\ u_{k+n,k+n} &= -A^* \end{aligned} \tag{2.4.5}$$

where $A = \sin(\phi_1)e^{i\phi_2}$ and $B = \cos(\phi_1)e^{i\phi_3}$. The total matrix U_e can be written as

$$U_e = \prod_{k=1}^{M-1} \prod_{n=1}^{M-k} U_{k,n} \tag{2.4.6}$$

the number of parameters on which a unitary matrix U_e acting on the extended space depends are $\frac{3M(M-1)}{2}$, belonging to $[0, 2\pi]$.

In condensed matter, a minimization method is often used to simulate the annealing of a material, which is then allowed to cool slowly; to repeat the process as necessary to remove impurities so that the system reaches its state of minimum magnetic energy. This algorithm is called simulated annealing (SA), and similarly to this process is where the parameterization of equation 2.4.5 is framed, where the three angles are used as an analog to solve the orientation of a magnetic moment in a two-dimensional space in condensed matter. In this manner, solving the minimization of the convex roof problem is equal to finding the configuration of angles $\vec{\phi}$ which minimizes the magnetic energy. In this thesis, instead of using the SA algorithm, we have used the freely available resources offered by Python. In particular, the library Scipy.optimize [36], which incorporates the basin-

hopping algorithm [37], which finds a global minimization through a local minimization procedure.

Chapter 3

DMRG

3.1 Summary

Numerical approximation techniques are necessary to solve problems in many areas of physics, especially when there is no analytical solution. In particular, the study of one-dimensional chains involves the tensor product of multiple Hilbert spaces, resulting in dimensions impossible to simulate exactly for a classical computer if we want to model anything from a few tens of particles to near the thermodynamic limit. Here comes the relevance of the Density Matrix Renormalization Group (DMRG) algorithm [38], which nicely balances truncating the total Hilbert space of a spin chain to an effective dimension achievable by a classical computer, without sacrificing good accuracy in the results.

The key idea of the DMRG is to find a good basis representation to describe the system as its length increases[39]. As will be seen later, this occurs via the reduced density matrix of the blocks implementing an appropriate truncation of the Hilbert space.

This chapter describes the DMRG algorithm, both the infinite and finite cases..

3.2 Infinite system DMRG

Suppose we are searching for the ground state of a Hamiltonian of a general 1D chain. The Hamiltonian is composed of sites interacting with their neighbors and each site lives in a Hilbert space of dimension D. The Hamiltonian of the system can be written in a general way as

$$H = \sum_i \sum_q \left(J(q)\hat{A}_i(q)\hat{B}_{i+1}(q) + g(q)\hat{V}_i \right) , \tag{3.2.1}$$

where $J(q)$ and $g(q)$ are coupling constant, while $\{\hat{A}_i(q)\}_q$, $\{\hat{B}_i(q)\}_q$ and $\{\hat{V}_i(q)\}_q$ are sets of operators acting on the i-th site. The q-index is used to reference the different elements of these

sets [40].

In the majority of cases, the main objective of the infinite algorithm is to simulate a chain long enough for quantities such as energy per site or the mean value of local operators to converge without significant edge effects. However in our case, in addition, we can use the convergence of quantum correlations which has been reported to be an important improvement of DMRG to succeed in comparison with numerical renormalization [41].

The algorithm starts by defining a subsystem called block, composed of one site and the relevant operators acting on it. In the literature, the block is often denoted as $B(L, m_{kept})$ [40]; the arguments refer to the number of sites L that contain and the number of states to describe it. Next, the *enlarged-block* (EB) is formed by considering the interaction terms between the block and a free site adjacent to the right. Because of the importance of the order in the tensor products is that the previous EB is called *Left enlarged-block* (LEB). The Hamiltonian of the LEB can be read as

$$\hat{H}_{LEB} = \hat{H}_B + \hat{H}_S + \hat{H}_{BS} \tag{3.2.2}$$

this Hamiltonian is composed of the Hamiltonians of the block $\hat{H}_B$, the site $\hat{H}_S$, and the interaction between them $\hat{H}_{BS}$. It is important to remark that in the first step, the block Hamiltonian only includes local terms. The operators that affect the LEB are also written enlarged, making the tensor product between the identity matrix of the LEB and the operators of the block

$$\hat{A}_{LEB} = \mathbf{I} \otimes \hat{A} \tag{3.2.3}$$

The next step is to form the *superblock*, by considering the interaction between the LEB with the *Right enlarged-block* (REB). The REB is a structure similar to the LEB, except the block is now on the right and the free site is adjacent to its left side. The Hamiltonian of the superblock is

$$\hat{H}_{SB} = \hat{H}_{LEB} + \hat{H}_{REB} + \hat{H}_{LR} \tag{3.2.4}$$

here we have the Hamiltonians of each EB and their interaction $\hat{H}_{LR}$. This super Hamiltonian describes the total $B(L, m_{kept})$-site-site-$B(L, m_{kept})$ system. At this point, we can obtain the ground state $|\Phi_0\rangle$, by diagonalizing equation 3.2.4; and use it to construct the density matrix of the chain, as indicated in equation 2.2.10

$$\rho = |\Phi_0\rangle \langle\Phi_0| \tag{3.2.5}$$

next step is to obtain the reduced density matrix of the LEB (REB),

$$\rho_{LEB} = tr_{REB} \left(|\Phi_0\rangle \langle\Phi_0| \right) \tag{3.2.6}$$

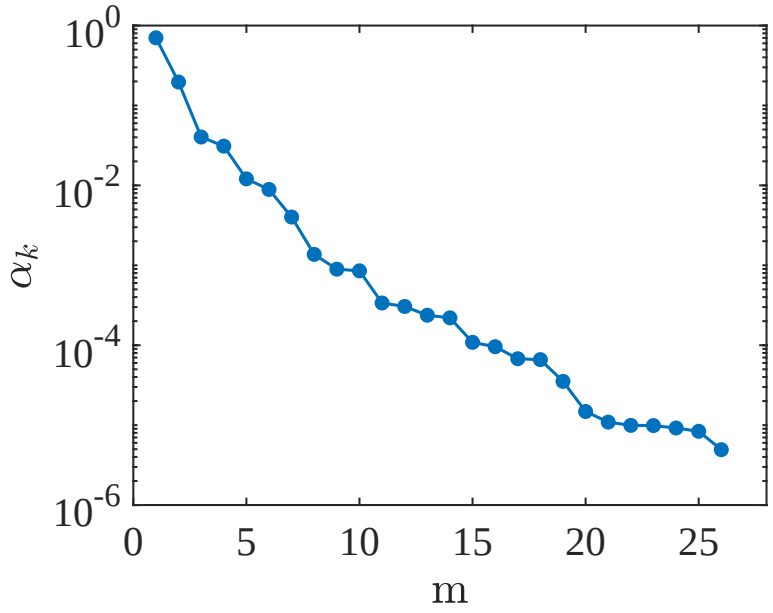

Figure 3.1: Eigenvalue spectrum of the reduced density matrix of a block for the case $(\Delta, D) = (0.15, -2)$ $m = 26$ and 1500 sites. On the y-axis, we have the eigenvalues with the highest value, while on the x-axis they are ordered in decreasing order.

at this point, it is necessary to employ the (pre-fixed) number m of states to truncate the Hilbert space. The dimension of the enlarged block $d_{EB} = D\, d_{block}$ is compared with this number

$$m_{kept} = min(d_{EB}, m) \tag{3.2.7}$$

and the minimum value between those is chosen to select the most relevant m_{kept} eigenstates of the reduced density matrix of the LEB (REB). The most relevant eigenstates are the ones with larger amplitude, and are used to construct the matrix of change of basis O_L (O_R), such that the new block Hamiltonian is written in the new representation of "absorbing" a central cite,

$$\hat{H}'_{LEB} = O_L^{\dagger}\, \hat{H}_{LEB}\, O_L \tag{3.2.8}$$

and similarly, other block operators are renormalized

$$\hat{A}'_{LEB} = O_L^{\dagger}\, \hat{A}_{LEB}\, O_L$$

finally, the new LEB (REB) and block operators are renamed for the algorithm to repeat by adding two central sites between the renormalized EBs. The process is repeated until the system reaches a certain size or the precision of the results is under a specified tolerance.

The number of fixed states m must be at least greater than the dimension of one site D and should also be selected so that the algorithm yields good results. To achieve good results we may

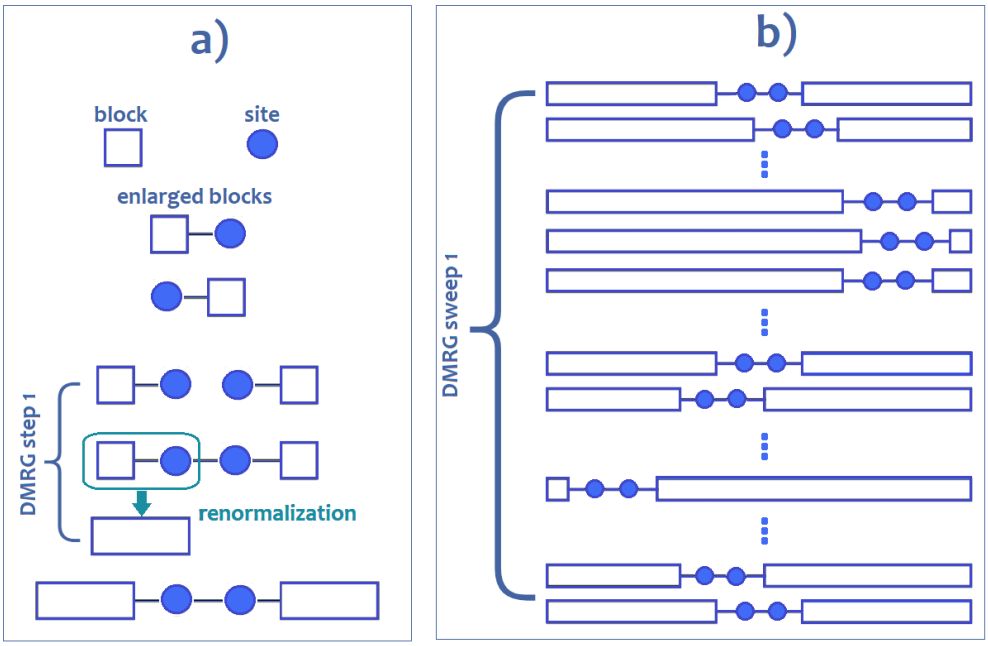

Figure 3.2: Schematic process of DMRG algorithm [40]. On subpanel a) one iteration of the infinite process is shown. On the left panel b), is illustrated one sweep in the finite algorithm.

look at the truncation error, that is, the error made for discarding all eigenvalues besides the m more relevant,

$$\epsilon_{tr} = \sum_{i>m} \lambda_i \tag{3.2.9}$$

where λ_i are the eigenvalues of the reduced density matrix of the EB in decreasing order. The equation 3.2.9 can be rewritten considering the property that the trace of the density matrix adds to one

$$\epsilon_{tr} = 1 - \sum^{m} \lambda_i \tag{3.2.10}$$

This approximation is good when the eigenvalues of the reduced density matrix of one of the EB decrease quickly, such that it is distinguishable the main contribution of the eigenstates α_k with larger eigenvalues in comparison with the eigenstates with eigenvalues closer to zero, as shown in figure 3.1. In this case, one can choose a number that keeps the quickly decreasing behavior of these eigenvalues, if there is such behavior.

The summarized steps of the infinite DMRG algorithm, illustrated in panel a) of figure 3.2, are outlined below:

1. Build the operator matrices for a single site Hamiltonian, and the operators involved in the interaction terms between this site and the rest of the system. With this, we form the initial blocks denoted as *B(1,D)*.

2. Grow each block with one site to form the LEB and REB. Also, write the interaction operators in the enlarged form.

3. Construct the superblock, find the ground state, and build the density matrix of the chain.

4. Obtain the reduced density matrix for each EB. Compare the EB dimension with m and evaluate if truncation is needed according to equation 3.2.7. Then obtain these most relevant eigenstates of the reduced density matrices and form the matrices O_L and O_R

5. Renormalized all relevant operators to go from $B(L, m_{kept})$ to new blocks $B(L+1, m_{kept})$ and repeat the process from step 2.

An important comment to make is related to the diagonalization process. At the first steps the system is small enough to perform exact diagonalization, but as the size increment until truncation is needed, one may prefer to use a more optimal method, especially considering that only one eigenstate is required, the ground state. That is the reason is highly suggested to accomplish this task with a library routine, such as Lanczos or Davidson algorithm. [39]

3.3 Finite system DMRG

Despite the fact that the infinite method obtains good results in general, there are cases where the required accuracy will not be obtained, for example, if there are impurities in the Hamiltonian or there is a very large magnetic field that traps the system in a metastable state in the first steps of DMRG when the edge effects are not negligible [39, 40]. The finite method solves these problems by means of so-called sweeps. Although we will not use this method in this thesis, we consider it valuable to mention the main idea.

The algorithm starts with a warm-up process, using the infinite DMRG algorithm until a maximum superblock size L_{max} is reached. This length is preserved constant. After that, one block $B(L_{max}/2 - 1, m)$ increases its size absorbing one central site forming the block $B(L_{max}/2, m)$, while the other block releases a site and shorts its length as $B(\frac{L_{max}}{2} - 2, m)$, such that two central sites are always maintained between the blocks. The block that is enlarged, remains increasing its size until the block that is shortened contains only one site $B(1, D)$, and then the process is carried out inversely, extending the block until the other block contains only one site. This process is called sweeping and is responsible for obtaining the convergence of the results. A scheme of this step is on part b) of the figure 3.2.

Chapter 4

Quantum phase transitions in spin chains

4.1 Summary

Spin chains are interesting systems for understanding many-body physics, because they represent an initial approximation to the many-body problem, without losing the relative simplicity of a one-dimensional model. In this chapter, we will present the concept of quantum phase transition (QPT) and the classification criteria according to the traditional view, and the correspondence with the quantum correlation perspective. In this chapter, the basic aspects of spin algebra will be introduced. Then, a short review of the spin $\frac{1}{2}$ models known in the literature and their QPTs will be made, to finally address the spin 1 model on which this work is focused.

4.2 What is a quantum phase transition

To define what a quantum phase transition is, we will go back to defining what a phase is and how one can move from one phase to another. To address this problem, let us start by talking about many-body physics. The great thing about many-body physics lies not so much in the number of bodies being studied but in the interactions between them. It is well-known how to solve an isolated particle problem, considering a collection of these would be the same as solving N times the same problem. The interactions between a large collection of particles result in states of matter with measurable and distinguishable properties at the macroscopic level. In statistical mechanics, the main purpose is to write the partition function of a system. This is related to the free energy, which at the same time is related to the thermodynamic quantities of the system by the orders of derivatives in the energy with respect to some parameter of the Hamiltonian describing the system.

We call the state of a many-body system with well-defined physical quantities a phase [42]. When there is a phase transition, some physical properties of the system change to new ones, and is common to use a distinctive property as an order parameter to characterize the phase transition. This change is associated with a singular behavior in energy [1, 2]. Since for a finite set of particles, the energy is always continuous, we have to speak of non-analytic behavior in the energy only in the thermodynamic limit. In other words, a phase transition occurs only in a system where the number of particles tends to infinity. As to how a phase transition occurs, it is simply obtained by varying a parameter of control that affects the system until it reaches a point close to a transition, where fluctuations at the microscopic level become relevant. Commonly, phase transitions are usually caused by variations in temperature, such as boiling a kettle or cooling a ferromagnetic material. However, when we talk about a quantum phase transition, temperature ceases to play a relevant role since QPTs occur at zero temperature. This implies two things, first, that the system is in its ground state, and second, that quantum fluctuations are responsible for the QPT rather than thermal fluctuations.

4.2.1 Classification criteria

Although the types of phase transitions are varied, in this thesis work we will limit ourselves to those related to non-analytic behavior at some order of the ground state energy derivatives. Thus, a first-order QPT (1QPT) is related to a discontinuity in the first derivative of the ground state energy. Similarly, a second-order QPT (2QPT) is related to a discontinuity or divergence in the second derivative of the ground state energy.

The names of these classifications come from historical reasons linked to Ehrenfest's classification. Even though this classification contained an error, formally nowadays 1QPT are generally defined as those transitions where there is associated latent heat, and 2QPT or continuous phase transitions, as they are called since the error in the old classification has been corrected, are characterized by exhibiting a critical behavior near a transition point, where a decay power law governs the correlations, the correlation length is infinite and hence the susceptibility diverges.

Despite the usual classification through energy, the link between QPTs and Quantum information theory allows us to take advantage of a correspondence between the traditional classification and the quantum correlations present in the ground state. In this way, Wu, Sarandy, and Lidar [43] demonstrate that for Entanglement measures, a discontinuity in a correlation estimator indicates a 1QPT, while a discontinuity or divergence in the first derivative of the correlation estimator indicates a 2QPT. The latter has also proven true for QD in the Dillenschneider paper [13], and other articles where QD has spotlighted QPT [15–17]. In [17], Malvezzi detects a 2QPT as an inflection point in QD in the spin 1 Heisenberg model.

4.3 Spin algebra

To define the algebra of any spin $\hat{S} = (S^x, S^y, S^z)$, 2 elements are needed [44]. Firstly, the commutation relation between its components

$$[S^\alpha, S^\beta] = i\epsilon_{\alpha\beta\gamma} S^\gamma \tag{4.3.1}$$

and second, the realization of the operators on an orthonormal basis. The spin operators act on a Hilbert space of dimension 2S+1, which we denote $\{|\psi^m\rangle\}$,

$$\begin{aligned} S^z |\psi^m\rangle &= m |\psi^m\rangle \\ S^\pm |\psi^m\rangle &= \sqrt{S(S+1) - m(m \pm 1)} \left|\psi^{m\pm 1}\right\rangle \end{aligned} \tag{4.3.2}$$

We assume $\hat{S}^2 = S(S+1)\mathcal{I}$, where S is the spin number. This number can take integer or half-integer values of the form $n/2$, with $n = 1, 2, 3, ...$ For m, this value goes from $-S$ to S, changing by one unit at a time, or in another equivalent representation, from 0 to $2S$, whether is used the traditional way or the computational basis to write $\{|\psi^m\rangle\}$.

The basis has a vector representation, traditionally chosen to be the eigenstates of S^Z. The basis state can be written as a column vector full of zeros, except for one entry with a value of one. In this work, we will use the computational basis states [31]. For determining the vectorial form, the index of the row that contains the 1 will be the same which indicates the value of m, starting from 0 to the position $2S$.

$$|\psi^m\rangle = \begin{pmatrix} 0 \\ 0 \\ ... \\ 1 \\ 0 \\ ... \\ 0 \end{pmatrix} \tag{4.3.3}$$

For the case of spin $\frac{1}{2}$, the eigenstates of S^z and spin operators are

$$S^x = \frac{1}{2}\begin{pmatrix} 0 & 1 \\ 1 & 0 \end{pmatrix}, \quad S^y = \frac{i}{2}\begin{pmatrix} 0 & -1 \\ 1 & 0 \end{pmatrix}, \quad S^z = \frac{1}{2}\begin{pmatrix} 1 & 0 \\ 0 & -1 \end{pmatrix} \tag{4.3.4}$$

$$|0\rangle = \begin{pmatrix} 1 \\ 0 \end{pmatrix} \qquad |1\rangle = \begin{pmatrix} 0 \\ 1 \end{pmatrix} \tag{4.3.5}$$

It should be noted that for $\frac{1}{2}$ the spin operators can be represented in terms of Pauli matrices as $\sigma^\alpha = 2S^\alpha$, $\alpha = x, y, z$

For the case of spin 1, the eigenstates of S^z and spin operators are

$$S^x = \frac{1}{\sqrt{2}}\begin{pmatrix} 0 & 1 & 0 \\ 1 & 0 & 1 \\ 0 & 1 & 0 \end{pmatrix}, \quad S^y = \frac{i}{\sqrt{2}}\begin{pmatrix} 0 & -1 & 0 \\ 1 & 0 & -1 \\ 0 & 1 & 0 \end{pmatrix}, \quad S^z = \begin{pmatrix} 1 & 0 & 0 \\ 0 & 0 & 0 \\ 0 & 0 & -1 \end{pmatrix} \tag{4.3.6}$$

$$|0\rangle = \begin{pmatrix} 1 \\ 0 \\ 0 \end{pmatrix} \qquad |1\rangle = \begin{pmatrix} 0 \\ 1 \\ 0 \end{pmatrix} \qquad |2\rangle = \begin{pmatrix} 0 \\ 0 \\ 1 \end{pmatrix} \tag{4.3.7}$$

These matrix and base representations will be used throughout the thesis.

4.4 Spin 1/2

4.4.1 Transverse XY and Ising models

The Hamiltonian of the anisotropic XY model consists of an N $\frac{1}{2}$-spin chain with nearest neighbor interaction immersed in an external magnetic field, given by

$$H = -\sum_i^N \left(J(\frac{(1+\gamma)}{2}\sigma_i^x\sigma_{i+1}^x + \frac{(1-\gamma)}{2}\sigma_i^y\sigma_{i+1}^y) + h\sigma_i^z \right) \tag{4.4.1}$$

where $\sigma^\alpha, \alpha = x, y, z$ are the Pauli matrices, J is the exchange interaction parameter, h is the intensity of the magnetic field and γ is the amount of anisotropy in the spin-spin interaction restricted at the xy-plane. Here $|\gamma| < 1$. Defining the dimensional coupling constant $\lambda = \frac{J}{2h}$ is convenient.

This model encompasses two other well-known models [45]. When $\gamma = 1$, the equation 4.4.4 becomes the Hamiltonian for the transverse field Ising model

$$H = -\sum_i^N (J\sigma_i^x\sigma_{i+1}^x + h\sigma_i^z) \tag{4.4.2}$$

this model is the subject of a 2QPT for a critical magnetic field value at $h_c = 1$. The system is in a ferromagnetic ordered phase with magnetization $\langle\sigma^x\rangle \neq 0$ for $h < h_c$, and in a paramagnetic disordered phase with $\langle\sigma^x\rangle = 0$ for $h > h_c$. Moreover, for the interval $0 < \gamma \leq 1$ in equation 4.4.4, the model belongs to the Ising universality class and undergoes the same 2QPT for h_c [45, 46].

When $\gamma = 0$, the equation 4.4.4 becomes the Hamiltonian for the isotropic transverse XY model

$$H = -\sum_{i}^{N} \left(J(\frac{1}{2}\sigma_i^x \sigma_{i+1}^x + \frac{1}{2}\sigma_i^y \sigma_{i+1}^y) + h\sigma_i^z \right) \tag{4.4.3}$$

this model also has a QPT called anisotropic transition, which divides the regime where $\gamma > 0$ where the magnetization is in the x-axis, from $\gamma < 0$, where the magnetization is in the y-axis. For the case of $\gamma = 0$ and $h = h_c$, there is no ferro-paramagnetic transition, but instead an insulator-metal -like 2QPT exists with no symmetry order parameter. This is called a Lifshitz transition [46].
This model has an analytical solution using the Jordan-Wigner transform [47], which is a transformation that maps the spin system to a fermion system. This transformation was applied to the XY model in the paper by Lieb et al. [48].

4.4.2 XXZ Heisenberg model

The Hamiltonian for the XXZ Heisenberg model consists of an N $\frac{1}{2}$-spin chain with nearest neighbor interaction in the 3 directions x,y,z

$$H = -\sum_{i}^{N} \left(S_i^x S_{i+1}^x + S_i^y S_{i+1}^y + \Delta S_i^z S_{i+1}^z \right) \tag{4.4.4}$$

where $S^\alpha, \alpha = x, y, z$ are the spin operators, related to Pauli matrices as $\sigma^\alpha = 2S^\alpha$ as stated in section 4.3. The anisotropy parameter in the z spin-spin interaction is Δ. This model has 2 critical points, for $\Delta_{c1} = -1$ where a 1QT take place, and $\Delta_{c2} = 1$ where the system undergoes a 2QPT. The system is in the ferromagnetic Ising phase for the range $\Delta < \Delta_{c1}$. In the interval $\Delta_{c1} < \Delta < \Delta_{c2}$ the system is in the XY phase, and finally for $\Delta > \Delta_{c2}$, the system is in the Néel or antiferromagnetic phase [45]. The analytical solution for the antiferromagnetic case was given for Bethe, with the Bethe ansatz [49].

4.5 Spin 1

4.5.1 XXZ Heisenberg model with single-ion anisotropy

The Hamiltonian that describes the one-dimensional spin 1 Heisenberg model with uniaxial single-ion anisotropy is

$$H = \sum_{i}^{N} \left\{ \left(\hat{S}_i^x \hat{S}_{i+1}^x + \hat{S}_i^y \hat{S}_{i+1}^y + \Delta \hat{S}_i^z \hat{S}_{i+1}^z \right) + D \left(\hat{S}_i^z \right)^2 \right\} \tag{4.5.1}$$

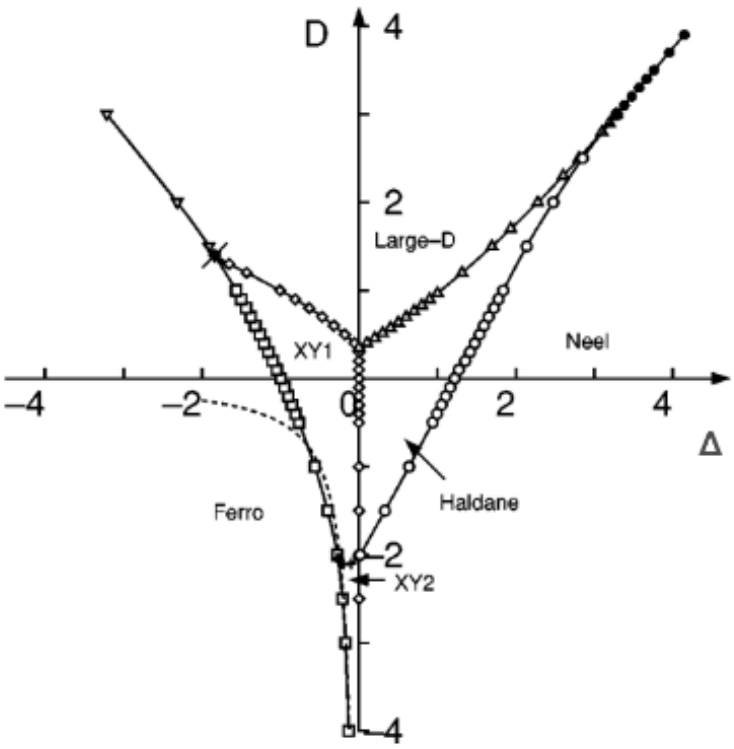

Figure 4.1: Phase diagram of S1 XXZ model with single-ion anisotropy, equation 4.5.1. Figure taken from Chen et al. [50].

where N is the total number of sites, $\hat{S}_i^\alpha$ are spin 1 operators from section 4.3. The parameter Δ characterizes the anisotropy between the spin exchange interaction in the z-axis of the system, and D is the uniaxial single-ion anisotropy.

For the case of $D = 0$, we recover the S-1 XXZ Heisenberg model. The phases through which this model is divided are well established [51, 52], the first critical point $\Delta_{c1} = -1$ divides the ferromagnetic phase (left) from the XY phase (right) through a 1QPT, see figure 4.1 for $D = 0$. The second transition point at $\Delta_{c2} \approx 0$ divides de XY phase from the Haldane phase through a Berezinskii–Kosterlitz–Thouless (BKT) transition. This transition is of infinite order, i.e., it does not imply a discontinuity in any order of the ground state derivative, nor is related to a broken symmetry, evenmore is a topological phase transition. This phase extends until the third critical point $\Delta_{c3} \approx 1.185$, which signals the 2QPT from the Haldane phase to the Néel phase. It is important to remark that Δ_{c2} and Δ_{c3} have been consensual through numerical results [52]. A relevant feature of this model is that it has a symmetry point $\mathcal{SU}(2)$ at $\Delta = 1$ where the model is isotropic. Although this model already exhibits greater richness as a higher spin model compared to the spin 1/2 models, by adding a uniaxial anisotropy term D, we obtain an even more complex and abundant phase diagram, see figure 4.1, because, in addition to the phases above mentioned, we add a new one, the large-D phase.

The new phase transitions from the single-ion anisotropy term are the Haldane-Large-D topological phase transition and the infinite order BKT transition between the XY-Large-D phases. The ferromagnetic to Large-D 1QPT transition and the Large-D to Néel transition, which nature is still unknown, although it is believed to be a 1QPT [50, 53].

Concerning order parameters, both the ferromagnetic and Néel phases have magnetic order. In the ferromagnetic phase, all the spins point in the same direction, this evidenced by the spin-spin correlation $\langle S_i^z S_{i+1}^z \rangle$, while in the Néel phase, all the nearest-neighbor spins are aligned in the opposite direction. This is characterized by the Néel order parameter $(-1)^n \langle S_i^z S_{i+1}^z \rangle$. On the other hand, the Haldane phase has a non-local topological string order parameter $-\langle S_i^z e^{i\pi \sum_{k=i+1}^{j-1} S_j^z} S_j^z \rangle$[53].

Chapter 5

Results

5.1 Summary

In this chapter, we present the results obtained in this thesis. The approach we implemented to study QPTs in the spin-1 chain is essentially numerical. As we have mentioned in the preceding chapters, DMRG method is the appropriate method to study the fundamental state of this system. On the other hand, quantum correlations as an estimator of QPTs must be calculated appealing to an optimization calculation. In the first instance, we will present calculations of some previous results found in the literature, and some new results concerning the calculation of quantum correlations in high-dimensional systems. Among the results we present the calculation of QD for an incoherent superposition of maximally entangled states in dimensions 2, 3, and 4, and also the calculation of QD for a two-qutrit system at finite temperature. Finally, we will show in detail calculations of quantum correlations in spin chains. In particular in those systems described in chapter 4.

5.2 Optimization results

Within the quantum world, there exists a zoology of relevant states such as Bell states, usually known as EPR states. These states play an essential role in the development of quantum theory since the crucial work by Einstein, Podolsky, and Rosen [24], where fundamental issues such as the nonlocal nature of quantum mechanics were questioned. Bell states embody the essential ingredient of quantum correlations since they exhibit maximal entanglement and maximal quantum discord.

Bell states for a couple of qubits (spin $\frac{1}{2}$) can be conveniently written as

$$\begin{aligned} |\Phi_{\pm}\rangle &= \frac{1}{\sqrt{2}}(|00\rangle \pm |11\rangle) \\ |\Psi_{\pm}\rangle &= \frac{1}{\sqrt{2}}(|01\rangle \pm |10\rangle) \end{aligned} \tag{5.2.1}$$

Bell states can be generated using the Hadamard and CNOT gates for qubits. Although famous, these are not the only maximally entangled states. We can use the same protocol used for qubits to produce maximally entangled states in higher dimensions. It should be noted the process for generating entanglement in principle depends on the quantum discrete Fourier transform and a conditional operation. For the case of qubits, the quantum discrete Fourier transform returns the Hadamard gate. The conditional operation, in our case defined as a function of the modular addition, yields the CNOT gate. The details of this procedure and calculation of maximally entangled states for qubits and higher dimensional systems are discussed in the appendix A.1.

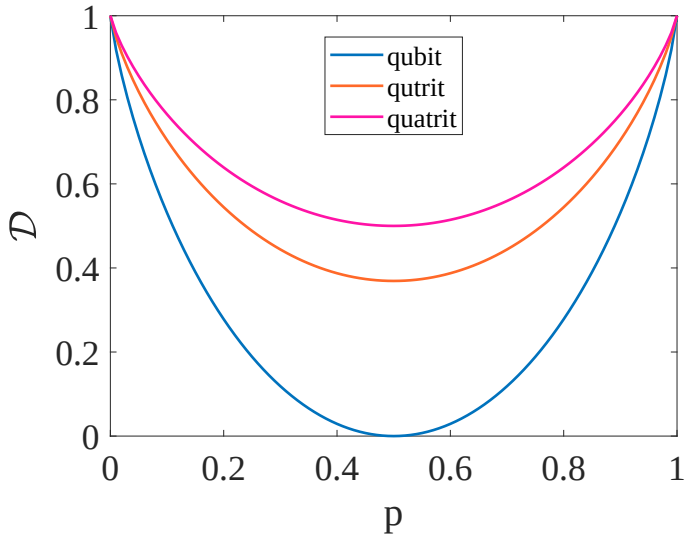

Figure 5.1: Quantum Discord computed for an incoherent superposition of maximally entangled states, for the cases of dimension 2, 3, and 4.

To test the performance of our optimization algorithm, we consider incoherent superpositions between two maximally entangled states for qubit, qutrits, and quatrits. The number of states for each case is d^2, with $d = 2$ for qubits, $d = 3$ for qutrits, and $d = 4$ for quatrits. Let us choose a particular incoherent superposition as follows

$$\rho_d = p\left|v^d\right\rangle\left\langle v^d\right| + (1-p)\left|v_{\perp}^d\right\rangle\left\langle v_{\perp}^d\right| \tag{5.2.2}$$

where p plays the role of the mixing probability, varying in the interval $[0, 1]$, $\{\left|v^d\right\rangle\}$ are the

maximally entangled states for dimension d. Intuitively this kind of state should exhibit minimal correlations for a balanced superposition, where the mixture is equal.

To study the quantum correlations of these systems, we calculate the QD for ρ_2, ρ_3 y ρ_4. For each case, the logarithms in entropies at the calculation of QD were normalized to the corresponding dimension d of the system, so the maximum value of QD is one for each curve. Observing the figure 5.1, it is evident that quantum correlations are symmetric for $p = 0.5$, where the minimum of quantum correlation is localized, as we thought for a balanced incoherent superposition. Particularly for the case of qubits, we notice that when the superposition is balanced the minimum of QD is zero, which does not occur when we perform the superpositions for higher dimensions. Notably, the minimum value of QD grows as the dimension of the system under study increases. Another thing to note is that the curves have the same behavior in the extreme cases where $p = 0$ or $p = 1$, producing the maximum correlation in both cases, which is trivially explained by having just one of the two maximally quantum correlated states that conform ρ_d, with maximal QD. It is also important to say the general behavior of the curves in figure 5.1 does not change depending on which states $|v^d\rangle$ and $|v^d_\perp\rangle$ we choose to superpose. We should mention that, when writing this thesis, we were unaware these results had been studied in the literature.

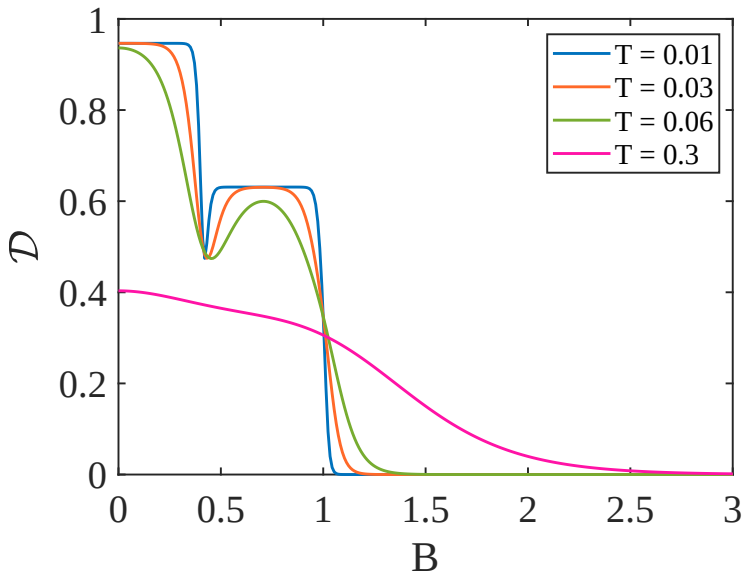

Figure 5.2: Quantum Discord computed for finite temperatures in a bipartite qutrit system, in function of an external magnetic field.

Moving to the second result used to test the performance of the optimization algorithm, in figure 5.2 we were able to reproduce some results obtained in the article by Hou et al. [54]. In that work, they focused on studying the quantum correlations of a two-qutrit system with exchange

interaction J in the presence of a magnetic field B at finite temperatures

$$H = J(S_{1x}S_{2x} + S_{1y}S_{2y}) + B(S_{1z}S_{2z}) \tag{5.2.3}$$

In the paper, they first obtained the eigenstates $\{|\psi_i\rangle\}$ and eigenvectors E_i of the Hamiltonian written above. Then, they wrote the state in thermal equilibrium according to the canonical ensemble

$$\rho_{eq} = \frac{1}{\mathcal{Z}} \sum_i e^{\frac{E_0 - E_i}{k_B T}} |\psi_i\rangle \langle\psi_i| \tag{5.2.4}$$

where $\mathcal{Z}$ is the partition function. We performed the correlation calculations with the explicit form of ρ_{eq}. Again, in the computation of QD, the logarithms in entropies were normalized to $d = 3$, which explains the difference at scale in the y-axis in figure 5.2 compared with the original paper where the calculations were made in qubit base. Also, J and k_B were set to 1 during the calculation.

As a result, the QD was obtained as a function of the magnetic field at a finite temperature. Observing figure 5.2, in the temperature range $T = 0.01 - 0.06$ there is a sharp change in QD at $B \approx 4$. At that point, in the limit $T \to 0$, the system has three different ground states, which would indicate signs of a QPT if the thermodynamic limit of the system were considered. For the case of $T = 0.3$, we observe fewer quantum correlations and the curve decays smoothly unlike the previous cases. We can also see that there is a maximum value of the magnetic field that can be applied before QD decays to 0 and this value increases with temperature.

In both cases studied we found satisfactory results to rely on our optimization algorithm. We advanced the results to estimate the QPTs in spin chains.

5.3 DMRG results

The process of applying the algorithm to spin chains is exemplified in the appendix B.1, where it is used in the principal model studied in this thesis, the Hamiltonian of the XXZ Heisenberg model with a single-ion anisotropy, described by the equation 4.5.1.

Among all the figures of merit studied in the chapter 2 to quantify the quantum correlations of various systems, we were faced with discriminating between them when studying the applicability to different models. Since exists a Concurrence relation for qubits, we directly used that relation instead of performing an unnecessary optimization process for calculating entanglement. For spin-1 the number of parameters to be optimized in the Eof case amounted to 108, considering $M = 9$ and the number of parameters $\frac{3M(M-1)}{2}$, as mentioned in chapter 2. Because of the expense of this optimization process, we decided to discard using Eof to characterize the QPTs of the spin-1 XXZ model with single-ion anisotropy, and instead rely on negativity when necessary.

On the other hand, at the QD calculation level, we had to decide when to calculate it depending on the particular model we were dealing with, specifically talking about spin-1/2 chains. Some systems demanded a higher amount of computational resources than others, even though they are systems of dimension 2, which was mentioned in chapter 3 as a consequence of the growth of entanglement. This was the case for the spin-1/2 XXZ model. So, in honor of time, we only calculated the QD of some of them. Fortunately for the spin-1 case, the optimization of the QD calculation could be performed pleasingly, with a parameter space of dimension $\frac{3\times3\times(3-1)}{2} = 9$. Thus, this correlation estimator was the bastion to calculate the phase diagram of our spin-1 system.

To ensure the reliability of our results, we use the truncation error and the convergence of the quantum correlations at the critical points, where these quantities become smaller the farther from a QPT. The first was given in chapter **??**, and we also averaged this quantity for the last 100 sites in order to obtain a mean value as a representation of the total truncation error for the simulation. And the second is based on examining the convergence of Concurrence per site (computed at each DMRG step increasing the size of the chain) in the spin-1/2 case, or the convergence of "naive Concurrence" per site in the spin-1 case. The latter naive estimator is explained in the spin-1 results section. With these general comments clarified, we proceed to present the spin 1/2 results.

5.3.1 Spin 1/2

Considering the case-by-case of each model, the parameters used to perform the simulation of a spin chain by DMRG, such as the number of sites L or the number of eigenstates kept m vary for each one, mainly taking care to maintain a low truncation error and to ensure the convergence of the quantum correlations.

For the first figure 5.3 the Concurrence obtained for the Ising model in a transverse field is observed, in agreement with the results obtained by Osenda, et al [55]. For this model, a chain with $L = 1000$ sites and $m = 14$ was simulated. In all spin-1/2 chains, we set $h = 1$ and varied J, such that in the dimensional coupling λ, the critical point translates into $\lambda_c = 0.5$. The truncation error is of the order 10^{-8} and the convergence of the Concurrence per site is of the order of 10^{-6}. In this case, the peak of quantum correlation is not related to a QPT, but the change of concavity observed at the critical point $\lambda_c = 0.5$ evidence the occurrence of a 2QPT, which is supported by the second derivative of the energy per site in figure 5.4. For the calculation of QD, the result is still pending because of the obstacle of being a quantity that requires greater precision compared to the Concurrence in this case around the 2QPT.

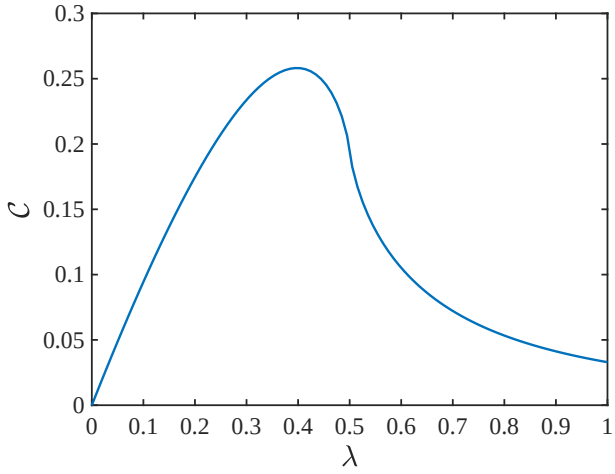

Figure 5.3: Concurrence calculated for the TFIM. The transition point is located at $\lambda_c = 0.5$. The maximum in the correlation does not relate quit the QPT. The curve was simulated with $L = 1000$ sites and $m = 14$ states of truncation.

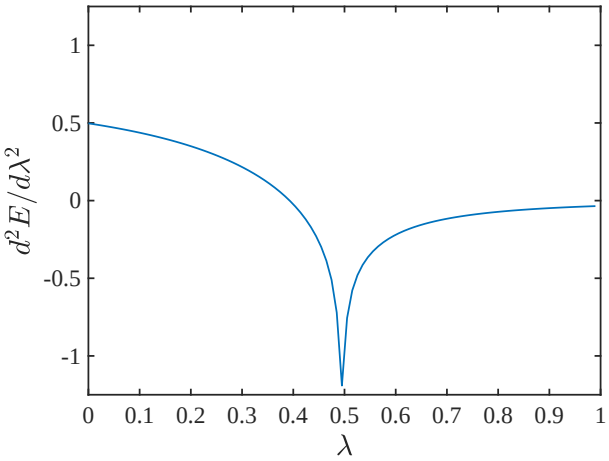

Figure 5.4: Second derivative of the energy per site in the TFIM. This figure shows the evidence of a 2QPT en $\lambda_c = 0.5$.

In the case of the transverse XY model, the spin chain was simulated with $L = 1000$ sites and $m = 16$. The truncation error is of the order 10^{-9} and the convergence of the Concurrence per site is of the order of 10^{-6}. We can observe the Concurrence of this model in figure 5.5, which is also consistent with the results of Osenda et al [55]. The 1QPT of the model can be pointed out in the abrupt discontinuity in the quantum correlation at $\lambda_c = 0.5$, dividing the two phases present in the model. For the case of QD in figure 5.3, we observe it also indicates the QPT at λ_c, following the same tendency as the Concurrence.

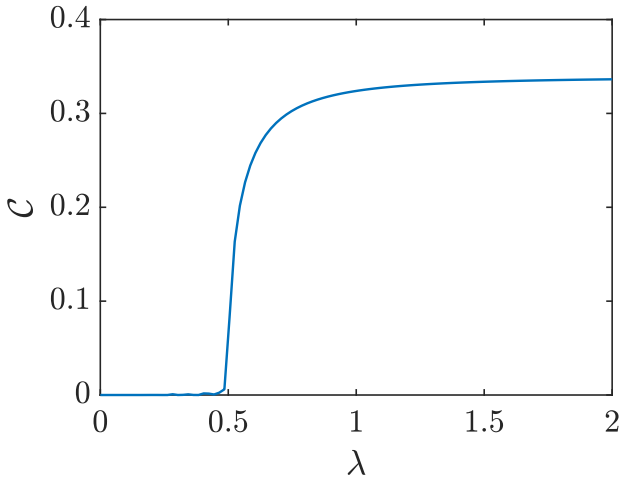

Figure 5.5: Concurrence for the isotropic XY transversal model. The transition point for the 1QPT is located at $\lambda_c = 0.5$. The curve was simulated with $L = 1000$ sites an $m = 16$ states of truncation

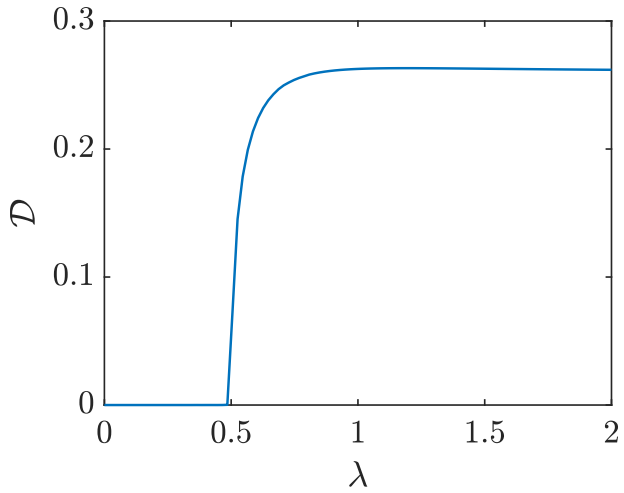

Figure 5.6: Quantum discord for the isotropic XY transversal model. It signals de transition point at $\lambda_c = 0.5$.

Finally, we have the Concurrence for the Heisenberg XXZ spin 1/2 model in figure 5.7. Unlike Ising's model, here the 2QPT coincides with the correlation maximum at $\Delta_c = 1$, and on the other hand, the 1QPT is evident at the discontinuity when $\Delta_c = -1$. For this model, we divided de computation into two parts due to the demanding convergence. The first part was simulated with $L = 2000$ and $m = 14$ in the range $\Delta \in [-1.8, 0)$, where the truncation error is of the order of 10^{-9} and the convergence of Concurrence per site is of the order of 10^{-6}.

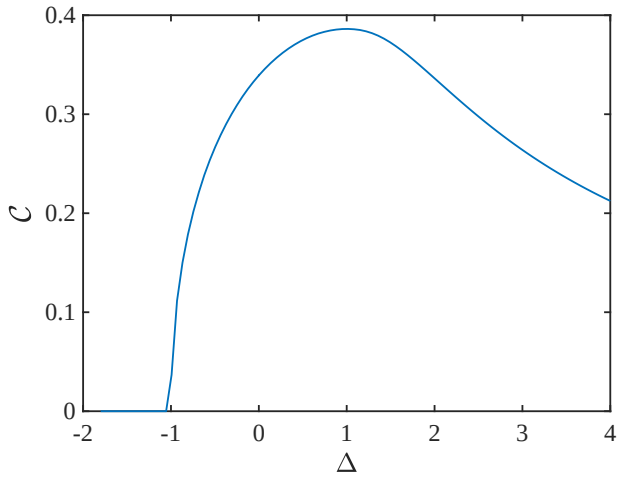

Figure 5.7: Concurrence for the XXZ model. This model has two transition points, one is located at $\Delta = -1$, with a 1QPT. And the second point is located at the maximum value of correlation, $\Delta = 1$, where a 2QPT occurs. The curve was simulated in parts, due to convergence difficulties.

The second and most difficult part was simulated with $L = 10000$ sites and $m = 16$ in the range $\Delta \in [0, 4]$. Even with these parameters, the sector between $\Delta \in \approx [0.7, 1.2]$ failed to converge to a satisfactory order. Given this, to obtain the curve in the figure 5.7 we use the fact that the convergence of the Concurrence per site oscillates between two values, which in the optimal case are shortening in distance from each other until we reach approximately the averaged value. We calculate this average by hand and replace it in the Concurrence as the final value. The optimal choice would be to provide more Hilbert space and sites to converge the simulation, but for time constraints we chose this qualitative approach that managed to show this 2QPT, as can be contrasted in the paper of Dillenschneider [13]. Since the mean value of the Concurrence does not change the lack of convergence in the density matrices of the central sites, we cannot calculate the QD of this model until we obtain the converged simulation with the correct parameters.
The computed quantum correlations correctly replicate the literature results, pointing out the QPTs of these spin chains. This allows us to ensure the reliability of our DMRG algorithm for studying QPTs in higher dimensions. Even for the case of the spin 1/2 XXZ model, we can ensure this since the motive for the no convergence in the difficult range is a resource issue rather than an error in the DMRG algorithm issue.

5.3.2 Spin 1

We finally present the main result of this work. The QPTs for the spin-1 XXZ Heisenberg model with single-ion anisotropy, that we studied numerically using QD as the principal estimator, and Negativity to compare in particular cases. The parameters to perform the simulation in different intervals of (Δ, D) had to be chosen after initial trials where the truncation error, the accuracy of

the energy per site, and the convergence of the quantum correlations were ensured. In general, all phase transition curves were calculated using QD, and only in some distinct cases were compared with negativity. An essential point for the numerical work was to use a naive correlation estimator to study the convergence of quantum correlations. As we explained in chapter 2, there is no analytical expression for Concurrence or Eof in dimensions higher than qubits, and optimizing 108 angles for each trial and error until we found the pair (L, m) that minimized the truncation error was out of the question. However, in an occurrence prompted by curiosity and necessity, the Wooters' Concurrence expression with spin 1 operators was used to calculate this naive analog of Concurrence in a higher dimension, such that it would serve as a guide to evaluate the convergence of the quantum correlations and facilitate finding the (L, m) parameters for which the data were reliable. This method in no way counts as proof of a generalization to higher dimensions of Concurrence. However, it is neither silly nor entirely wrong to calculate this quantity, since it is related to the observable S^y and hence has to carry some information. So, recognizing its naive character, this method was used to ensure the convergence of the quantum correlations.

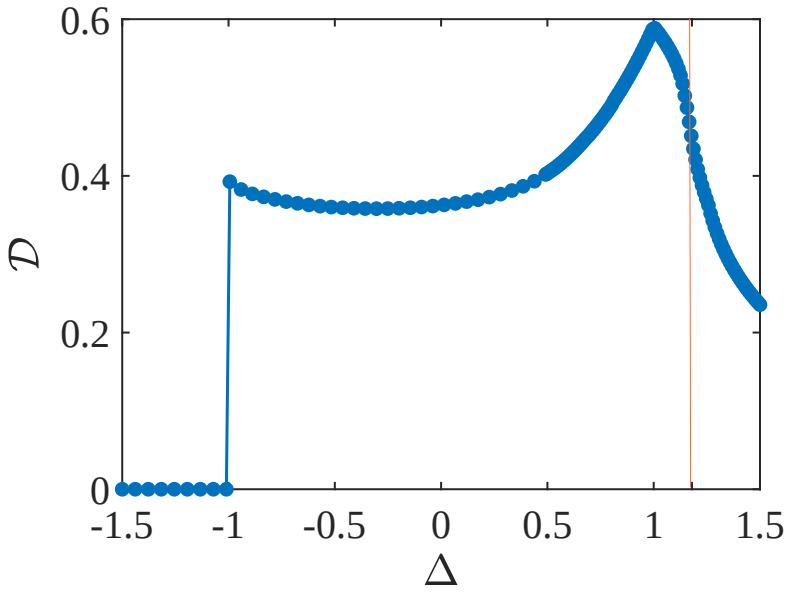

Figure 5.8: Quantum discord versus the anisotropy parameter Δ in the spin-1 XXZ model. From left to right, the first discontinuity signals a 1QPT at $\Delta = -1$. The peak is not a QPT, but a symmetry point. At the light orange is demarked the 2QPT around $\Delta_c \approx 1.18$.

First, we present the result with $D = 0$, where the general model reduces to the spin-1 Heisenberg XXZ system. For this case, we managed to reproduce the result of the work of Malvezzi, et al. [17] by finding the QD curve in the interval of $\Delta \in [-1.5, 1.5]$. For this particular curve, the QD was calculated by intervals, and with the entropies in qubit basis. The sections are 3, $\Delta \in [-1.50, -1.01]$, $\Delta \in [-0.99, 0.49]$ and $\Delta \in [0.5, 1.5]$. In the first interval, the data was obtained

with $L = 500$ and $m = 14$. In the second, the parameters of the simulation were $L = 100$ and $m = 16$, and the final interval was simulated with $L = 100$ and $m = 24$. The difference between these parameters is explained by understanding that there are zones within the same curve where the simulation converges quickly compared to the others. The latter is a zone of difficult convergence of quantum correlations, which requires a greater balance with respect to Hilbert space to truncate in the DMRG algorithm. Sometimes, like this one, increasing the Hilbert space considerably helps to the point of not having to simulate such a long chain. In principle, it would be ideal to let the DMRG algorithm automatically regulate itself in terms of L and m, just delivering the desired tolerance and letting the program run until the output condition is met. However, this approach has the disadvantage of being very expensive for the computer, and also that if there is any point of high entanglement there may be no convergence at a high tolerance, and must be addressed in another way, such as with finite DMRG.

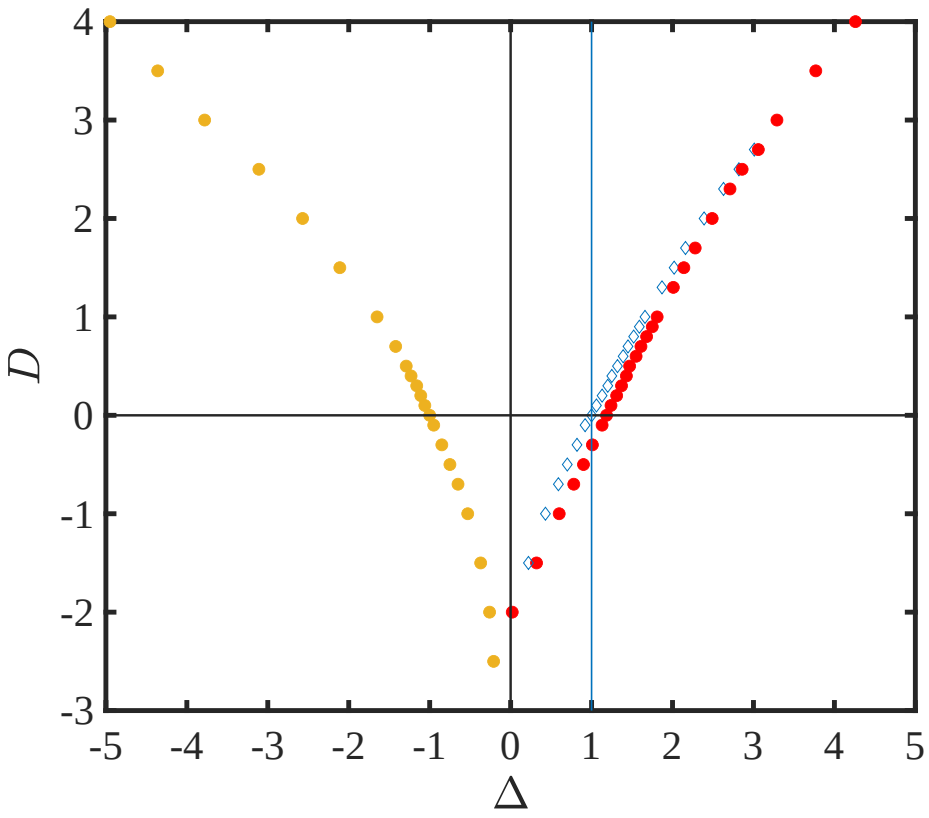

Figure 5.9: Numerical phase diagram of the S-1 XXZ Heisenberg model with single-ion anisotropy, constructed with Quantum Discord for the ferromagnetic (white dots) and Néel (red dots) curve transition, in addition, there is a line characterizing the symmetry point of $(\Delta, D) = (1, 0)$ (diamond markers) as D varies.

We can observe from the figure 5.8 that the 1QPT from ferro to XY phase is clearly observed

at $\Delta_c = -1$, and the same is true for the 2QPT evidenced by the change of concavity around $\Delta_c = 1.18$. The symmetry point at $\Delta = 1$ is also visible. For the case of the BKT transition at $\Delta \approx 0$, there is no indication in the QD that could point to this phase transition. This is in line with what was mentioned in chapter 4, where the infinite order character of this transition was mentioned, plus the fact the order parameter for the Haldane phase is non-local.

Turning to results with $D \neq 0$, we focus on finding the first- and second-order phase transitions, since as mentioned above, QPT outside the traditional classification must be addressed with different tools. In particular, for topological QPT between the Haldane and Large-D phases, we believe that we must extend our study to next-neighbor correlations at least since the local character of the quantum correlations we study in this work does not allow us to approach this type of special transition. In this way, we manage to reproduce the ferromagnetic and antiferromagnetic or Néel transition curves, plus a novel curve characterizing the change of the symmetry point (SP) at $(\Delta, D) = (1, 0)$ as D is varied. The general diagram was introduced in chapter 4, and we can contrast it with our result in figure 5.9.

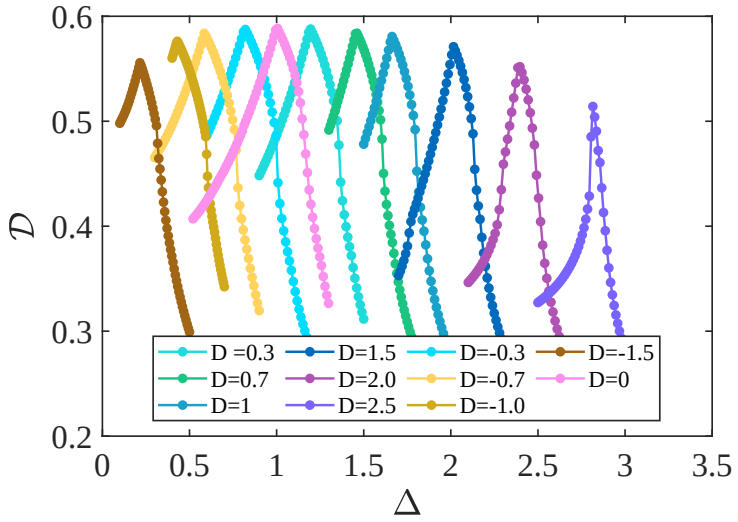

Figure 5.10: Close up of Quantum discord for the symmetry point (peaks) and 2QPT sector, as the single-ion anisotropy D term is varied. The case $(\Delta, D) = (1, 0)$ is illustrated at the pink curve. The Δ coordinate of the peaks for each curve is taken and represents the blue curve with diamond markers in figure 5.9.

In the case of the ferromagnetic curve, for the simulation of the chain in the DMRG algorithm, we use $L = 1500$ sites and $m = 18$ eigenstates, with the only difference being the case for $D = 0$, where the data have already been mentioned above. The convergence for the energy per site for this curve ranges between $10^{-7} - 10^{-8}$, while the correlation of the naive Concurrence varies for each point between $10^{-5} - 10^{-9}$. The error associated with the truncation process it is shown in table 5.1, where they are displayed on a scale of 10^{-6}.

In the case of the Néel curve, it was necessary to simulate some sectors more accurately than others. For $D \in [4, 3]$ we used $(m, L) = (18, 1500)$, while for $D \in [2.7, 0.1]$ we used $(m, L) = (18, 3500)$. Finally for $D \in [-0.1, -1.5]$ we use $(m, L) = (18, 1500)$, and in particular for $D = -2$ the parameters were $(m, L) = (26, 1500)$. The convergence of the energy in all the cases just mentioned, both for the SP and the QPT curves, is of the order of 10^{-8}, and for the convergence of the naive Concurrence it ranges between $10^{-7} - 10^{-9}$ in the SP, while for the QPT it ranges between $10^{-6} - 10^{-9}$. In particular at $D = -2$ for the SP curve, the convergence of the naive Concurrence is of the order of 10^{-5}. Regarding the truncation error, in table 5.2 we can see it on a scale of 10^{-5}.

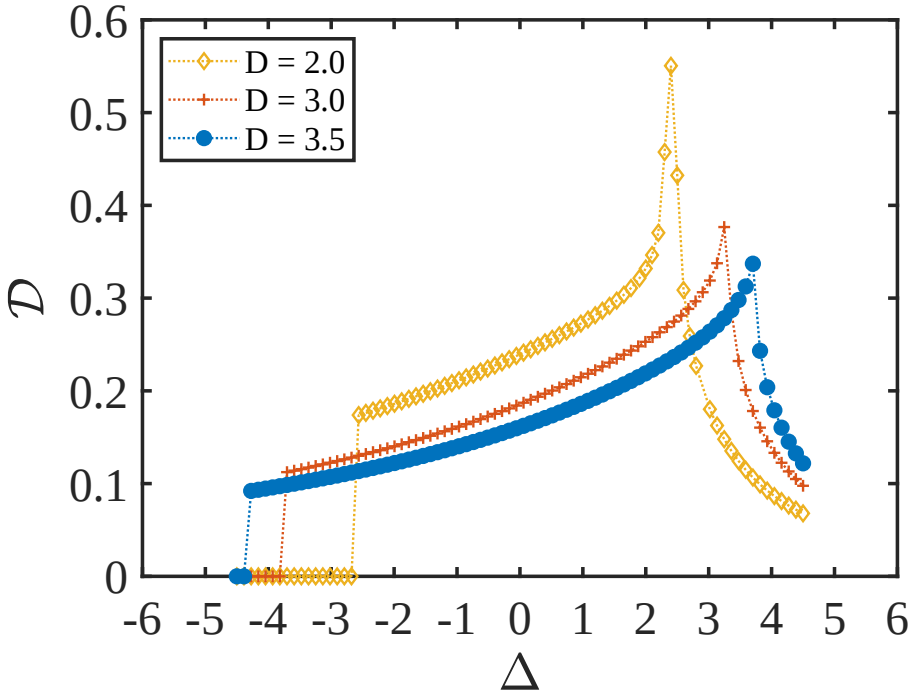

Figure 5.11: Quantum discord for the cases of $D = 2, 3, 3.5$. For $D = 2$ in the region $\Delta > 0$ we are in the region where there is still a 2QPT, unlike the other two values, where the Néel-Large-D transition occurs. At the left, where $\Delta < 0$ it can be observed the 1QPT of each curve.

In order to understand the phase diagram in figure 5.9, we found it relevant to have some curves that maintain a full extension in Δ to cover the two QPTs. Thus in figure 5.10 we can observe the change in the peak of the symmetry point as D varies. In figures 5.11 and 5.12 we can see the behavior of the QD and Negativity for the cases $D = 2, 3, 3.5$. It is clear to notice that the ferromagnetic 1QPT is distinguished as a discontinuity in both correlation estimators. While for the Néel phase curve, for $D = 3, 3.5$ we have a sharp change in QD, but for Negativity a discontinuity in the function becomes present. For $D = 2$ we observe a smooth behavior of change in Negativity, while for QD it is difficult to distinguish at first glance a concavity change in the figure, but it is

known to be there thanks to calculations and can be better contemplated in the figure 5.10. This supports the evidence for a 2QPT.

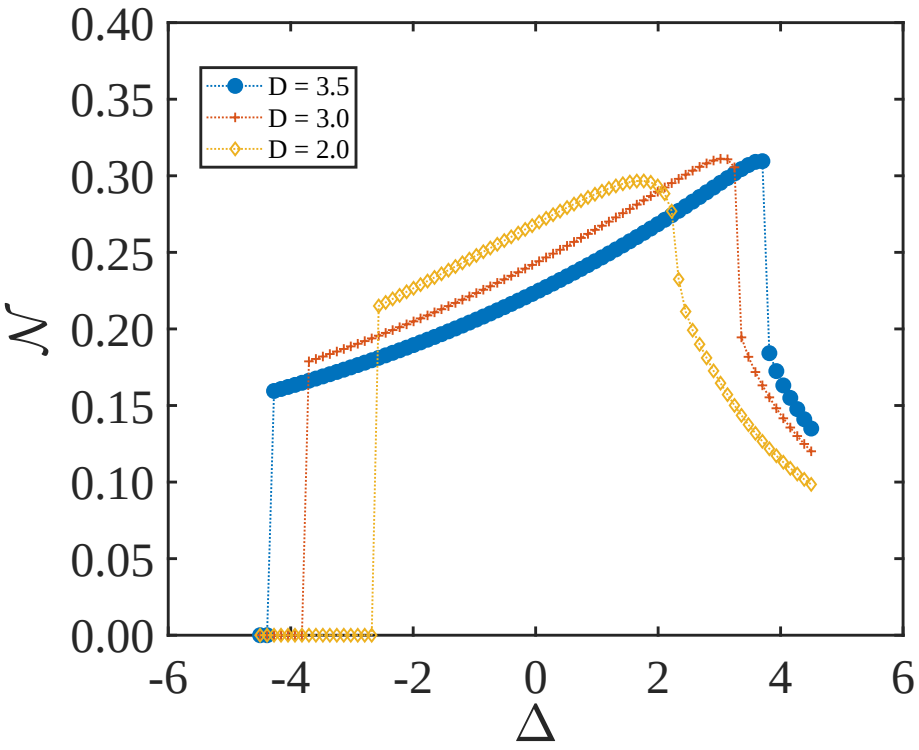

Figure 5.12: Negativity for the cases od $D = 2, 3, 3.5$. We can observe in the ferromagnetic region that Negativity exhibits a discontinuity where the 1QPT is located. In the other extreme, for $D = 2$ we have a smooth behavior in comparison with the discontinuities presented for the other cases. This is consistent with what is shown in figure **??**.

For comparison, we have also calculated the energy per site for these cases, and also for the $D = 0.5, 1$ cases, see figure 5.13. In particular for the antiferromagnetic curve at $D = 0.5, 1, 2$ we also have a smooth change in energy. This change in energy agrees with that exhibited in Negativity, both of which evidence the 2QPT present if the derivative of these quantities is taken, by observing an inflection point in them. Considering the other cases of $D = 3, 3.5$ we can see a sharp change in energy, which agrees with the behavior of Negativity and QD at the néel curve. And exactly, the same behavior is observed in the 1QPT in the ferromagnetic transition sector for those D.

Some relevant things to mention after finishing the numerical work are the following. The quantum correlations do not necessarily have the maximum of their correlations at the transition point, as we could see in this spin-1 model, as well as in the Ising model and the XY with a transverse field. The XXZ spin-1/2 model is the exception in this work. We believe that it is precisely due to this occurrence that we faced a difficult convergence for the two central sites.

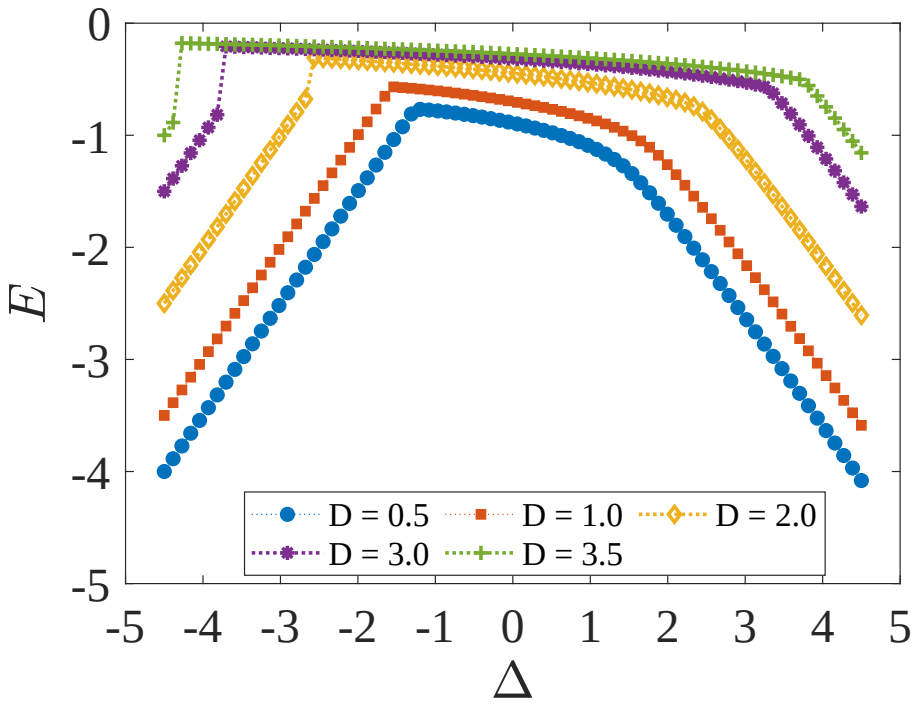

Figure 5.13: Energy per size vs *Delta* for the cases of $D = 2, 3, 3.5$. In this figure, we have 5 different curves. All of them show a sharp break behavior in the 1QPT at *Delta* < 0, but on the other hand in the *Delta* > 0 sector the curves with $D = 0.5, 1, 2$ show smooth changes in the energy, which translates into a 2QPT if we look at the energy derivatives. For $D = 3, 3.5$ we have an abrupt change.

Related to the numerical aspects of the DMRG algorithm, a relevant detail is that having a convergent energy value does not necessarily relate to the same convergence accuracy of the local quantum correlations we study. This is curious because intuitively we might think that the above is a direct consequence. However, we see that this is not the case when comparing the columns of the tables 5.2 and 5.1 with the mentioned values of quantum correlation convergence.

To go a little further into the physics of this problem, we want to address the intuition of the ground state of the system in the ferro- and antiferromagnetic phases. In principle, this is straightforward for the state in the ferromagnetic phase if we imagine a system of qubits, as traditionally done since the condition that the spins remain aligned is still fulfilled. However, the topic gets a bit more interesting when we ask what an antiferromagnetic state means for spin-1. What characterizes an antiferromagnetic state in qubit systems is that there is zero net magnetization as a consequence of the antiparallel alignment between neighboring spins. This concept can be fully transferred to the spin-1 case, but without losing the consideration of the contribution of the subspace $m_z = 0$. Therefore, if we imagine a bipartite spin-1 system consisting of two sites, we have 3^2 states that describe the possible configuration of the system. Using as exceptional notation for each qutrit, the

Ferromagnetic transition curve.	
D	Truncation error $[10^{-6}]$
4.0	6.78×10^{-2}
3.5	1.01×10^{-2}
3.0	2.45×10^{-2}
2.5	9.78×10^{-2}
2.0	2.32×10^{-1}
1.5	2.15×10^{-1}
1.0	7.49×10^{-1}
0.7	7.08
0.5	8.71×10^{-2}
0.4	2.99×10^{-3}
0.3	2.44×10^{-4}
0.2	3.24×10^{-5}
0.1	6.38×10^{-6}
0.0	$x \times 10^{-2}$
-0.1	1.95×10^{-3}
-0.3	1.45×10^{-1}
-0.5	1.83×10^{-1}
-0.7	4.66×10^{-1}
-1.0	1.25×10^{-10}
-1.5	3.10
-2.0	8.30
-2.5	5.29

Table 5.1: In this table the truncation error calculated for each QD curve is ordered as D varies, for the 1QPT ferromagnetic transition. Note that the truncation error is already on the scale of 10^{-6}.

states $|-\rangle, |0\rangle, |+\rangle$ as the eigenstates with eigenvalues $m_z = -1, 0, 1$, the following state represents an antiferromagnetic spin-1 state

$$\frac{1}{\sqrt{3}}(|+-\rangle + |-+\rangle + |00\rangle) \tag{5.3.1}$$

One question we are left wondering when trying to think of the form of the above state is what it means for the ground state to be in a Large-D phase, too. At the moment what we can answer, is that since S_z^2 acts at only one site, when applied to the above-defined basis, the $|+\rangle$ and $|-\rangle$ states both have eigenvalue equal to 1 for this operator, while $|0\rangle$ has a 0 eigenvalue. So we can say that depending on the minimization of energy, it can favor the alignment on the z-axis, but without any particular orientation, or it can promote the $|0\rangle$ eigenstates. Which at first impression lead us to think in a state with magnetization in z direction different from zero, lower than that which could be found in the ferromagnetic phase.

Néel transition curve.		
D	Truncation error SP $[10^{-5}]$	Truncation error QPT $[10^{-5}]$
4.0	-	3.41×10^{-1}
3.5	-	9.75×10^{-1}
3.0	-	2.26
2.7	4.30	2.71×10^{-1}
2.5	3.87	2.15
2.3	2.57	1.29
2.0	1.53	5.99×10^{-1}
1.7	1.05	4.68×10^{-1}
1.5	8.76×10^{-1}	2.21×10^{-1}
1.3	7.51×10^{-1}	3.84×10^{-1}
1.0	6.33×10^{-1}	3.94×10^{-1}
0.9	6.10×10^{-1}	2.93×10^{-1}
0.8	5.97×10^{-1}	7.43×10^{-1}
0.7	5.80×10^{-1}	6.13×10^{-1}
0.6	5.90×10^{-1}	4.04×10^{-1}
0.5	5.90×10^{-1}	6.59×10^{-1}
0.4	6.12×10^{-1}	3.03×10^{-1}
0.3	6.20×10^{-1}	2.66×10^{-1}
0.2	6.68×10^{-1}	2.43×10^{-1}
0.1	7.03×10^{-1}	4.87×10^{-1}
0.0	x	$x \times 10^{-2}$
-0.1	7.38×10^{-1}	2.63×10^{-1}
-0.3	6.69×10^{-1}	3.06×10^{-1}
-0.5	6.41×10^{-1}	5.06×10^{-1}
-0.7	6.61×10^{-1}	3.91×10^{-1}
-1.0	8.51×10^{-1}	1.07
-1.5	2.42	1.93
-2.0	-	2.58

Table 5.2: In this table the truncation error calculated for each QD curve is ordered as D varies, for the 2QPT, the Néel-Large-D transition and the symmetric point. Note that the truncation error is already on the scale of 10^{-5}

Conclusions

The aim of this work has been to study quantum correlations and quantum phase transitions present in the Heisenberg XXZ model of spin-1 with single-ion anisotropy, for an infinite one-dimensional chain with open boundary conditions. This system was simulated using the infinite DMRG numerical technique to obtain the ground state of the system. Using quantum correlation estimators, the first- and second-order QPTs of the system were detected.

We revisited quantum phase transitions that characterize fundamental models in the condensed matter area, such as the transverse field model of the Ising model with its 2QPT, the transverse isotropic XY model with its 1QPT, and the Heisenberg XXZ model with its 1QPT and 2QPT, to test our computational power with the DMRG algorithm and the optimization program. Taking a slight deviation from the main objective, we have also studied pure quantum correlations in special states, such as maximally entangled states that were arranged in an incoherent superposition. This was performed not only for qubits but also for higher dimensions $d = 3$ and $d = 4$. In addition to the above, finite temperature correlations were studied for a bipartite system of qutrits in the presence of a magnetic field, reproducing previously published results [54]. This was fruitful for us to check that our numerical computational tools worked reliably. In the numerical aspect of the DMRG technique, we simulate the spin chain systems with our algorithm, using 3 different criteria to verify the correct simulation of the models. The three criteria are the convergence of the energy per site, the truncation error, and the convergence of the quantum correlations. The last is represented by the Concurrence in the spin-1/2 case and the naive Concurrence in the spin-1 case. Having established the basis for reliable numerical work, we detected the first and second-order quantum phase transitions for the spin-1 Heisenberg XXZ model with a single-ion anisotropy building up the phase diagram based on Quantum Discord, which represents the main original finding of this thesis, not previously studied in the literature. This result agrees with those found in references [12, 50] where a different approach was used. Additionally, we also characterized a new line in the phase diagram, corresponding to the symmetry point $(\Delta, D) = (1, 0)$, which can be seen in Figure 5.8. This result extends the result from Malvezzi et. al [17] and Yuste et. al [12], two papers that were our first approach to the problem. Unlike the work of Yuste [12], where they characterized the phase diagram only for $D \geq 0$ using Negativity in finite chains, our study

was performed in an infinite one-dimensional chain with open boundary conditions, extending the study also in the cases of $D < 0$ and using Quantum Discord. With this correlation estimator it is possible to appreciate the displacement of the peak at the symmetry point as D is varied.

Natural projections of this work would be to extend our study of quantum correlations to second neighbors, to deal with phase transitions involving non-local correlations. We also aim to study quantum correlations in finite systems with different boundary conditions. Another direction could be to consider different configurations, which could include not restricting ourselves to one-dimensional systems. In the strict sense of quantum correlations and quantum phase transitions, we are interested in simulating other higher spin models to employ our numerical computational tool, especially those that have been mainly studied by entanglement.

Bibliography

[1] Subir Sachdev. *Quantum Phase Transitions*. 2nd ed. Cambridge University Press, 2011. DOI: 10.1017/CBO9780511973765 (Cited on pages 1, 2, 24).

[2] Keith Benedict. "Understanding Quantum Phase Transitions, edited by Lincoln Carr". In: *Contemporary Physics* 53.4 (2012), pp. 365–366. DOI: 10.1080/00107514.2012.672462. eprint: https://doi.org/10.1080/00107514.2012.672462. URL: https://doi.org/10.1080/00107514.2012.672462 (Cited on pages 2, 24).

[3] M. E. Fisher. "SCALING, UNIVERSALITY AND RENORMALIZATION GROUP THEORY". In: (1982) (Cited on page 2).

[4] D. P. Landau. "Finite-size behavior of the Ising square lattice". In: *Phys. Rev. B* 13 (7 Apr. 1976), pp. 2997–3011. DOI: 10.1103/PhysRevB.13.2997. URL: https://link.aps.org/doi/10.1103/PhysRevB.13.2997 (Cited on page 2).

[5] Murty S. S. Challa, D. P. Landau, and K. Binder. "Finite-size effects at temperature-driven first-order transitions". In: *Phys. Rev. B* 34 (3 Aug. 1986), pp. 1841–1852. DOI: 10.1103/PhysRevB.34.1841. URL: https://link.aps.org/doi/10.1103/PhysRevB.34.1841 (Cited on page 2).

[6] Jiahao Xu, Shan-Ho Tsai, D. P. Landau, and K. Binder. "Finite-size scaling for a first-order transition where a continuous symmetry is broken: The spin-flop transition in the three-dimensional XXZ Heisenberg antiferromagnet". In: *Phys. Rev. E* 99 (2 Feb. 2019), p. 023309. DOI: 10.1103/PhysRevE.99.023309. URL: https://link.aps.org/doi/10.1103/PhysRevE.99.023309 (Cited on page 2).

[7] A. Osterloh, Luigi Amico, G. Falci, and Rosario Fazio. "Scaling of entanglement close to a quantum phase transition". In: *Nature* 416.6881 (Apr. 2002), pp. 608–610. ISSN: 1476-4687. DOI: 10.1038/416608a. URL: https://doi.org/10.1038/416608a (Cited on pages 3, 4).

[8] William K. Wootters. "Entanglement of Formation of an Arbitrary State of Two Qubits". In: *Phys. Rev. Lett.* 80 (10 Mar. 1998), pp. 2245–2248. DOI: 10.1103/PhysRevLett.80.2245. URL: https://link.aps.org/doi/10.1103/PhysRevLett.80.2245 (Cited on pages 3, 12).

[9] Tobias J. Osborne and Michael A. Nielsen. "Entanglement in a simple quantum phase transition". In: *Phys. Rev. A* 66 (3 Sept. 2002), p. 032110. DOI: 10.1103/PhysRevA.66.032110. URL: https://link.aps.org/doi/10.1103/PhysRevA.66.032110 (Cited on page 5).

[10] G. Vidal, J. I. Latorre, E. Rico, and A. Kitaev. "Entanglement in Quantum Critical Phenomena". In: *Phys. Rev. Lett.* 90 (22 June 2003), p. 227902. DOI: 10.1103/PhysRevLett.90.227902. URL: https://link.aps.org/doi/10.1103/PhysRevLett.90.227902 (Cited on page 5).

[11] H. T. Quan, Z. Song, X. F. Liu, P. Zanardi, and C. P. Sun. "Decay of Loschmidt Echo Enhanced by Quantum Criticality". In: *Phys. Rev. Lett.* 96 (14 Apr. 2006), p. 140604. DOI: 10.1103/PhysRevLett.96.140604. URL: https://link.aps.org/doi/10.1103/PhysRevLett.96.140604 (Cited on page 5).

[12] A Yuste, C Cartwright, G De Chiara, and A Sanpera. "Entanglement scaling at first order quantum phase transitions". In: *New Journal of Physics* 20.4 (Apr. 2018), p. 043006. DOI: 10.1088/1367-2630/aab2db. URL: https://dx.doi.org/10.1088/1367-2630/aab2db (Cited on pages 5, 46).

[13] Raoul Dillenschneider. "Quantum discord and quantum phase transition in spin chains". In: *Phys. Rev. B* 78 (22 Dec. 2008), p. 224413. DOI: 10.1103/PhysRevB.78.224413. URL: https://link.aps.org/doi/10.1103/PhysRevB.78.224413 (Cited on pages 5, 24, 37).

[14] Martin Hofmann, Andreas Osterloh, and Otfried Gühne. "Scaling of genuine multiparticle entanglement close to a quantum phase transition". In: *Phys. Rev. B* 89 (13 Apr. 2014), p. 134101. DOI: 10.1103/PhysRevB.89.134101. URL: https://link.aps.org/doi/10.1103/PhysRevB.89.134101 (Cited on page 5).

[15] T. Werlang, C. Trippe, G. A. P. Ribeiro, and Gustavo Rigolin. "Quantum Correlations in Spin Chains at Finite Temperatures and Quantum Phase Transitions". In: *Phys. Rev. Lett.* 105 (9 Aug. 2010), p. 095702. DOI: 10.1103/PhysRevLett.105.095702. URL: https://link.aps.org/doi/10.1103/PhysRevLett.105.095702 (Cited on pages 5, 14, 24).

[16] T. Werlang, G. A. P. Ribeiro, and Gustavo Rigolin. "Spotlighting quantum critical points via quantum correlations at finite temperatures". In: *Phys. Rev. A* 83 (6 June 2011), p. 062334. DOI: 10.1103/PhysRevA.83.062334. URL: https://link.aps.org/doi/10.1103/PhysRevA.83.062334 (Cited on pages 5, 14, 24).

[17] A. L. Malvezzi et al. "Quantum correlations and coherence in spin-1 Heisenberg chains". In: *Phys. Rev. B* 93 (18 May 2016), p. 184428. DOI: 10.1103/PhysRevB.93.184428. URL: https://link.aps.org/doi/10.1103/PhysRevB.93.184428 (Cited on pages 5, 24, 38, 46).

[18] Shi-Liang Zhu. "Scaling of Geometric Phases Close to the Quantum Phase Transition in the XY Spin Chain". In: *Phys. Rev. Lett.* 96 (7 Feb. 2006), p. 077206. DOI: 10.1103/PhysRevLett.96.077206. URL: https://link.aps.org/doi/10.1103/PhysRevLett.96.077206 (Cited on page 5).

[19] Shu Chen, Li Wang, Yajiang Hao, and Yupeng Wang. "Intrinsic relation between ground-state fidelity and the characterization of a quantum phase transition". In: *Phys. Rev. A* 77 (3 Mar. 2008), p. 032111. DOI: 10.1103/PhysRevA.77.032111. URL: https://link.aps.org/doi/10.1103/PhysRevA.77.032111 (Cited on page 5).

[20] Shi-Jian Gu, Shu-Sa Deng, You-Quan Li, and Hai-Qing Lin. "Entanglement and Quantum Phase Transition in the Extended Hubbard Model". In: *Phys. Rev. Lett.* 93 (8 Aug. 2004), p. 086402. DOI: 10.1103/PhysRevLett.93.086402. URL: https://link.aps.org/doi/10.1103/PhysRevLett.93.086402 (Cited on page 5).

[21] Yan-Chao Li and Hai-Qing Lin. "Quantum coherence and quantum phase transitions". In: *Scientific Reports* 6.1 (May 2016), p. 26365. ISSN: 2045-2322. DOI: 10.1038/srep26365. URL: https://doi.org/10.1038/srep26365 (Cited on pages 5, 14).

[22] Michael A. Nielsen and Isaac L. Chuang. *Quantum Computation and Quantum Information: 10th Anniversary Edition*. Cambridge University Press, 2010. DOI: 10.1017/CBO9780511976667 (Cited on pages 6, 8, 16).

[23] J. J. Sakurai and Jim Napolitano. *Modern Quantum Mechanics*. 2nd ed. Cambridge University Press, 2017. DOI: 10.1017/9781108499996 (Cited on page 10).

[24] A. Einstein, B. Podolsky, and N. Rosen. "Can Quantum-Mechanical Description of Physical Reality Be Considered Complete?" In: *Phys. Rev.* 47 (10 May 1935), pp. 777–780. DOI: 10.1103/PhysRev.47.777. URL: https://link.aps.org/doi/10.1103/PhysRev.47.777 (Cited on pages 11, 30).

[25] John Stewart Bell. *Speakable and Unspeakable in Quantum Mechanics: Collected Papers on Quantum Philosophy*. New York: Cambridge University Press, 2004 (Cited on page 11).

[26] Stuart J. Freedman and John F. Clauser. "Experimental Test of Local Hidden-Variable Theories". In: *Phys. Rev. Lett.* 28 (14 Apr. 1972), pp. 938–941. DOI: 10.1103/PhysRevLett.28.938. URL: https://link.aps.org/doi/10.1103/PhysRevLett.28.938 (Cited on page 11).

[27] Charles H. Bennett et al. "Teleporting an unknown quantum state via dual classical and Einstein-Podolsky-Rosen channels". In: *Phys. Rev. Lett.* 70 (13 Mar. 1993), pp. 1895–1899. DOI: 10.1103/PhysRevLett.70.1895. URL: https://link.aps.org/doi/10.1103/PhysRevLett.70.1895 (Cited on page 11).

[28] Peter W. Shor. "Polynomial-Time Algorithms for Prime Factorization and Discrete Logarithms on a Quantum Computer". In: *SIAM Journal on Computing* 26.5 (1997), pp. 1484–1509. DOI: 10.1137/S0097539795293172. eprint: https://doi.org/10.1137/S0097539795293172. URL: https://doi.org/10.1137/S0097539795293172 (Cited on page 11).

[29] G. Vidal and R. F. Werner. "Computable measure of entanglement". In: *Phys. Rev. A* 65 (3 Feb. 2002), p. 032314. DOI: 10.1103/PhysRevA.65.032314. URL: https://link.aps.org/doi/10.1103/PhysRevA.65.032314 (Cited on page 13).

[30] Asher Peres. "Collective tests for quantum nonlocality". In: *Phys. Rev. A* 54 (4 Oct. 1996), pp. 2685–2689. DOI: 10.1103/PhysRevA.54.2685. URL: https://link.aps.org/doi/10.1103/PhysRevA.54.2685 (Cited on page 13).

[31] Michał Horodecki, Paweł Horodecki, and Ryszard Horodecki. "Separability of n-particle mixed states: necessary and sufficient conditions in terms of linear maps". In: *Physics Letters A* 283.1 (2001), pp. 1–7. ISSN: 0375-9601. DOI: https://doi.org/10.1016/S0375-9601(01)00142-6. URL: https://www.sciencedirect.com/science/article/pii/S0375960101001426 (Cited on pages 13, 25).

[32] Harold Ollivier and Wojciech H. Zurek. "Quantum Discord: A Measure of the Quantumness of Correlations". In: *Phys. Rev. Lett.* 88 (1 Dec. 2001), p. 017901. DOI: 10.1103/PhysRevLett.88.017901. URL: https://link.aps.org/doi/10.1103/PhysRevLett.88.017901 (Cited on page 13).

[33] L Henderson and V Vedral. "Classical, quantum and total correlations". In: *Journal of Physics A: Mathematical and General* 34.35 (Aug. 2001), p. 6899. DOI: 10.1088/0305-4470/34/35/315. URL: https://dx.doi.org/10.1088/0305-4470/34/35/315 (Cited on page 13).

[34] B. P. Lanyon, M. Barbieri, M. P. Almeida, and A. G. White. "Experimental Quantum Computing without Entanglement". In: *Phys. Rev. Lett.* 101 (20 Nov. 2008), p. 200501. DOI: 10.1103/PhysRevLett.101.200501. URL: https://link.aps.org/doi/10.1103/PhysRevLett.101.200501 (Cited on page 14).

[35] S. Allende, D. Altbir, and J. C. Retamal. "Simulated annealing and entanglement of formation for $(n \bigotimes m)$-dimensional mixed states". In: *Phys. Rev. A* 92 (2 Aug. 2015), p. 022348. DOI: 10.1103/PhysRevA.92.022348. URL: https://link.aps.org/doi/10.1103/PhysRevA.92.022348 (Cited on page 14).

[36] Pauli Virtanen et al. "SciPy 1.0: Fundamental Algorithms for Scientific Computing in Python". In: *Nature Methods* 17 (2020), pp. 261–272. DOI: 10.1038/s41592-019-0686-2 (Cited on page 16).

[37] David J. Wales and Jonathan P. K. Doye. "Global Optimization by Basin-Hopping and the Lowest Energy Structures of Lennard-Jones Clusters Containing up to 110 Atoms". In: *The Journal of Physical Chemistry A* 101.28 (1997), pp. 5111–5116. DOI: 10.1021/jp970984n. eprint: https://doi.org/10.1021/jp970984n. URL: https://doi.org/10.1021/jp970984n (Cited on page 17).

[38] Steven R. White. "Density matrix formulation for quantum renormalization groups". In: *Phys. Rev. Lett.* 69 (19 Nov. 1992), pp. 2863–2866. DOI: 10.1103/PhysRevLett.69.2863. URL: https://link.aps.org/doi/10.1103/PhysRevLett.69.2863 (Cited on page 18).

[39] Adrian E. Feiguin. "The Density Matrix Renormalization Group and its time-dependent variants". In: *AIP Conference Proceedings* 1419.1 (Dec. 2011), pp. 5–92. ISSN: 0094-243X. DOI: 10.1063/1.3667323. eprint: https://pubs.aip.org/aip/acp/article-pdf/1419/1/5/12037601/5_1_online.pdf. URL: https://doi.org/10.1063/1.3667323 (Cited on pages 18, 22).

[40] Gabriele De Chiara, Matteo Rizzi, Davide Rossini, and Simone Montangero. "Density Matrix Renormalization Group for Dummies". In: *Journal of Computational and Theoretical Nanoscience* 5.7 (July 2008), pp. 1277–1288. DOI: 10.1166/jctn.2008.2564. URL: https://doi.org/10.1166/jctn.2008.2564 (Cited on pages 19, 21, 22).

[41] Tobias J. Osborne and Michael A. Nielsen. "Entanglement, Quantum Phase Transitions, and Density Matrix Renormalization". In: *Quantum Information Processing* 1.1 (Apr. 2002), pp. 45–53. ISSN: 1573-1332. DOI: 10.1023/A:1019601218492. URL: https://doi.org/10.1023/A:1019601218492 (Cited on page 19).

[42] E. Fermi. *Thermodynamics*. Dover Books on Physics Series. Prentice-Hall, Incorporated, 1937. ISBN: 9780486461540. URL: https://books.google.cl/books?id=NK19fmSOsQUC (Cited on page 24).

[43] L.-A. Wu, M. S. Sarandy, and D. A. Lidar. "Quantum Phase Transitions and Bipartite Entanglement". In: *Phys. Rev. Lett.* 93 (25 Dec. 2004), p. 250404. DOI: 10.1103/PhysRevLett.93.250404. URL: https://link.aps.org/doi/10.1103/PhysRevLett.93.250404 (Cited on page 24).

[44] H. Tasaki. *Physics and Mathematics of Quantum Many-Body Systems*. Graduate Texts in Physics. Springer International Publishing, 2020. ISBN: 9783030412654. URL: https://books.google.cl/books?id=IU7iDwAAQBAJ (Cited on page 25).

[45] Amit Dutta et al. *Quantum Phase Transitions in Transverse Field Spin Models: From Statistical Physics to Quantum Information*. Cambridge University Press, 2015. DOI: 10.1017/CBO9781107706057 (Cited on pages 26, 27).

[46] Rolando Somma, Gerardo Ortiz, Howard Barnum, Emanuel Knill, and Lorenza Viola. "Nature and measure of entanglement in quantum phase transitions". In: *Phys. Rev. A* 70 (4 Oct. 2004), p. 042311. DOI: 10.1103/PhysRevA.70.042311. URL: https://link.aps.org/doi/10.1103/PhysRevA.70.042311 (Cited on pages 26, 27).

[47] P. Jordan and E. Wigner. "Über das Paulische Äquivalenzverbot". In: *Zeitschrift für Physik* 47.9 (Sept. 1928), pp. 631–651. ISSN: 0044-3328. DOI: 10.1007/BF01331938. URL: https://doi.org/10.1007/BF01331938 (Cited on page 27).

[48] Elliott Lieb, Theodore Schultz, and Daniel Mattis. "Two soluble models of an antiferromagnetic chain". In: *Annals of Physics* 16.3 (1961), pp. 407–466. ISSN: 0003-4916. DOI: https://doi.org/10.1016/0003-4916(61)90115-4. URL: https://www.sciencedirect.com/science/article/pii/0003491661901154 (Cited on page 27).

[49] H. Bethe. "Zur Theorie der Metalle". In: *Zeitschrift für Physik* 71.3 AB (Mar. 1931), pp. 205–226 (Cited on page 27).

[50] Wei Chen, Kazuo Hida, and B. C. Sanctuary. "Ground-state phase diagram of $S = 1$ XXZ chains with uniaxial single-ion-type anisotropy". In: *Phys. Rev. B* 67 (10 Mar. 2003), p. 104401. DOI: 10.1103/PhysRevB.67.104401. URL: https://link.aps.org/doi/10.1103/PhysRevB.67.104401 (Cited on pages 28, 29, 46).

[51] Tôru Sakai and Minoru Takahashi. "Finite-Size Scaling Study of S=1 XXZ Spin Chain". In: *Journal of the Physical Society of Japan* 59.8 (1990), pp. 2688–2693. DOI: 10.1143/JPSJ.59.2688. eprint: https://doi.org/10.1143/JPSJ.59.2688. URL: https://doi.org/10.1143/JPSJ.59.2688 (Cited on page 28).

[52] Atsuhiro Kitazawa, Kiyohide Nomura, and Kiyomi Okamoto. "Phase Diagram ofS=1 Bond-Alternating XXZ Chains". In: *Phys. Rev. Lett.* 76 (21 May 1996), pp. 4038–4041. DOI: 10.1103/PhysRevLett.76.4038. URL: https://link.aps.org/doi/10.1103/PhysRevLett.76.4038 (Cited on page 28).

[53] Chon-Fai Kam and Yang Chen. "Genuine Tripartite Entanglement as a Probe of Quantum Phase Transitions in a Spin-1 Heisenberg Chain with Single-Ion Anisotropy". In: *Annalen der Physik* 534.4 (2022), p. 2100342. DOI: https://doi.org/10.1002/andp.202100342. eprint: https://onlinelibrary.wiley.com/doi/pdf/10.1002/andp.202100342. URL: https://onlinelibrary.wiley.com/doi/abs/10.1002/andp.202100342 (Cited on page 29).

[54] Xi-Wen Hou, Xiu-Fang Lei, and Bo Chen. "Thermal quantum and classical correlations in a two-qutrit system". In: *The European Physical Journal D* 67.5 (May 2013), p. 106. ISSN: 1434-6079. DOI: 10.1140/epjd/e2013-30730-5. URL: https://doi.org/10.1140/epjd/e2013-30730-5 (Cited on pages 32, 46).

[55] Omar Osenda, Zhen Huang, and Sabre Kais. "Tuning the entanglement for a one-dimensional magnetic system with anisotropic coupling and impurities". In: *Phys. Rev. A* 67 (6 June 2003), p. 062321. DOI: 10.1103/PhysRevA.67.062321. URL: https://link.aps.org/doi/10.1103/PhysRevA.67.062321 (Cited on pages 34, 35).

Appendices

Appendix A

Appendices of Chapter 2

A.1 Entanglement states generation protocoles

In this appendix, we will develop the main ingredients necessary to generate entangled bipartite states. As well-known entangled pairs can be generated for qubits, using the Hadamard gate and a conditional two-qubit gate. The Hadamard gate is defined as the transformation

$$H = \frac{1}{\sqrt{2}} \begin{bmatrix} 1 & 1 \\ 1 & -1 \end{bmatrix}$$

that transform qubit states according to

$$H|0\rangle = \frac{1}{\sqrt{2}}(|0\rangle + |1\rangle)$$
$$H|1\rangle = \frac{1}{\sqrt{2}}(|0\rangle - |1\rangle)$$

We also introduce the conditional operation, usually called CNOT gate, which can be conveniently defined in terms of the modular addition for binary numbers

$$|i\rangle|j\rangle \longrightarrow |i\rangle|i \oplus j\rangle \tag{A.1.1}$$

The conditionality is based on changing the state of the second qubit depending on the state of the first qubit. We denote this conditional operation going from qubit 1 to qubit 2 as C_{12}. This

operation transforms qubits states according to

$$|00\rangle \to |00\rangle$$
$$|01\rangle \to |01\rangle$$
$$|10\rangle \to |11\rangle$$
$$|11\rangle \to |10\rangle$$

Entangled Bell states are obtained by applying the operation $C_{12}H_1 |i\rangle_1 |j\rangle_2$.

$$\begin{aligned}
C_{12}H_1 |00\rangle &= C_{12}\frac{1}{\sqrt{2}}(|0\rangle + |1\rangle)|0\rangle = \frac{1}{\sqrt{2}}(|00\rangle + |11\rangle) \\
C_{12}H_1 |01\rangle &= C_{12}\frac{1}{\sqrt{2}}(|0\rangle + |1\rangle)|1\rangle = \frac{1}{\sqrt{2}}(|01\rangle + |10\rangle) \\
C_{12}H_1 |10\rangle &= C_{12}\frac{1}{\sqrt{2}}(|0\rangle - |1\rangle)|0\rangle = \frac{1}{\sqrt{2}}(|00\rangle - |11\rangle) \\
C_{12}H_1 |11\rangle &= C_{12}\frac{1}{\sqrt{2}}(|0\rangle - |1\rangle)|1\rangle = \frac{1}{\sqrt{2}}(|01\rangle - |10\rangle)
\end{aligned} \tag{A.1.2}$$

Higher dimensions such as spin 1 or $\frac{3}{2}$ maximally entangled states can also be generated following the same recipe for qubits. In such a case, we have to define a generalized Hadamard gate and conditional gate acting on qudits, instead of qubits. The generalization of the Hadamard gate is given by the quantum discrete quantum Fourier transform, which is defined as follows

$$F_N |x\rangle = \frac{1}{\sqrt{N}} \sum e^{\frac{2\pi i x k}{N}} |k\rangle \tag{A.1.3}$$

where N is the dimension of the associated qudit space, $|x\rangle$ is the state to which the transform is applied, and $|k\rangle$ is the set of qudit states into which the initial state is expanded. In particular, we observe that the Hadamard gate corresponds to the two-dimensional quantum Fourier transform F_2

$$F_2 |0\rangle = \frac{1}{\sqrt{2}}(|0\rangle + |1\rangle)$$
$$F_2 |1\rangle = \frac{1}{\sqrt{2}}(|0\rangle - |1\rangle)$$

For qutrits the F_3 reads as

$$F_3 = \frac{1}{\sqrt{3}} \begin{bmatrix} 1 & 1 & 1 \\ 1 & e^{i\beta} & e^{-i\beta} \\ 1 & e^{-i\beta} & e^{i\beta} \end{bmatrix}$$

where the phase $\beta = 2\pi/3$. The nine maximally entangled states for qutrits are

$$\begin{aligned}
C_{12}F_3\,|00\rangle &= \frac{1}{\sqrt{3}}(|00\rangle + |11\rangle + |22\rangle) \\
C_{12}F_3\,|01\rangle &= \frac{1}{\sqrt{3}}(|01\rangle + |12\rangle + |20\rangle) \\
C_{12}F_3\,|02\rangle &= \frac{1}{\sqrt{3}}(|02\rangle + |10\rangle + |21\rangle)
\end{aligned}$$

$$\begin{aligned}
C_{12}F_3\,|10\rangle &= \frac{1}{\sqrt{3}}(|00\rangle + e^{i\beta}\,|11\rangle + e^{-i\beta}\,|22\rangle) \\
C_{12}F_3\,|11\rangle &= \frac{1}{\sqrt{3}}(|01\rangle + e^{i\beta}\,|12\rangle + e^{-i\beta}\,|20\rangle) \\
C_{12}F_3\,|12\rangle &= \frac{1}{\sqrt{3}}(|02\rangle + e^{i\beta}\,|10\rangle + e^{-i\beta}\,|21\rangle)
\end{aligned}$$

$$\begin{aligned}
C_{12}F_3\,|20\rangle &= \frac{1}{\sqrt{3}}(|00\rangle + e^{-i\beta}\,|11\rangle + e^{i\beta}\,|22\rangle) \\
C_{12}F_3\,|21\rangle &= \frac{1}{\sqrt{3}}(|01\rangle + e^{-i\beta}\,|12\rangle + e^{i\beta}\,|20\rangle) \\
C_{12}F_3\,|22\rangle &= \frac{1}{\sqrt{3}}(|02\rangle + e^{-i\beta}\,|10\rangle + e^{i\beta}\,|21\rangle)
\end{aligned}$$

For dimension four we have the F_4 of the form

$$F_4 = \frac{1}{\sqrt{4}}\begin{bmatrix} 1 & 1 & 1 & 1 \\ 1 & i & -1 & -i \\ 1 & -1 & 1 & -1 \\ 1 & -i & -1 & i \end{bmatrix}$$

The sixteen maximally entangled states for quatrts are,

$$\begin{aligned}
C_{12}F_4\,|00\rangle &= \frac{1}{\sqrt{4}}(|00\rangle + |11\rangle + |22\rangle + |33\rangle) \\
C_{12}F_4\,|01\rangle &= \frac{1}{\sqrt{4}}(|01\rangle + |12\rangle + |23\rangle + |30\rangle) \\
C_{12}F_4\,|02\rangle &= \frac{1}{\sqrt{4}}(|02\rangle + |13\rangle + |20\rangle + |31\rangle) \\
C_{12}F_4\,|03\rangle &= \frac{1}{\sqrt{4}}(|03\rangle + |10\rangle + |21\rangle + |32\rangle)
\end{aligned}$$

$$
\begin{aligned}
C_{12}F_4\,|10\rangle &= \frac{1}{\sqrt{4}}(|10\rangle + i\,|11\rangle - |22\rangle - i\,|33\rangle)\\
C_{12}F_4\,|11\rangle &= \frac{1}{\sqrt{4}}(|01\rangle + i\,|12\rangle - |23\rangle - i\,|30\rangle)\\
C_{12}F_4\,|12\rangle &= \frac{1}{\sqrt{4}}(|02\rangle + i\,|13\rangle - |20\rangle - i\,|31\rangle)\\
C_{12}F_4\,|13\rangle &= \frac{1}{\sqrt{4}}(|03\rangle + i\,|10\rangle - |21\rangle - i\,|32\rangle)\\
C_{12}F_4\,|20\rangle &= \frac{1}{\sqrt{4}}(|00\rangle - |11\rangle + |22\rangle - |33\rangle)\\
C_{12}F_4\,|21\rangle &= \frac{1}{\sqrt{4}}(|01\rangle - |12\rangle + |23\rangle - |30\rangle)\\
C_{12}F_4\,|22\rangle &= \frac{1}{\sqrt{4}}(|02\rangle - |13\rangle + |24\rangle - |31\rangle)\\
C_{12}F_4\,|23\rangle &= \frac{1}{\sqrt{4}}(|03\rangle - |10\rangle + |20\rangle - |32\rangle)\\
C_{12}F_4\,|30\rangle &= \frac{1}{\sqrt{4}}(|00\rangle - i\,|11\rangle - |22\rangle + i\,|33\rangle)\\
C_{12}F_4\,|31\rangle &= \frac{1}{\sqrt{4}}(|01\rangle - i\,|12\rangle - |23\rangle + i\,|30\rangle)\\
C_{12}F_4\,|32\rangle &= \frac{1}{\sqrt{4}}(|02\rangle - i\,|13\rangle - |20\rangle + i\,|31\rangle)\\
C_{12}F_4\,|33\rangle &= \frac{1}{\sqrt{4}}(|03\rangle - i\,|10\rangle - |21\rangle + i\,|32\rangle)
\end{aligned}
$$

Now that we have an idea of what the maximally entangled states look like, a mixed state conformed by an incoherent superposition of these states is constructed to observe the behavior of the correlations,

$$\rho_d = p\left|v^d\right\rangle\left\langle v^d\right| + (1-p)\left|v^d_\perp\right\rangle\left\langle v^d_\perp\right| \tag{A.1.4}$$

here p plays the role of the mixing probability, varying in the interval $[0,1]$. The maximally entangled states for dimension d are $\{\left|v^d\right\rangle\}$.

Appendix B

Appendices of Chapter 3

B.1 Infinite DMRG in Heisenberg model

This section presents the treatment of the Hamiltonian in equation 4.5.1 for the purposes of the DMRG algorithm.

The Hamiltonian of the spin 1 XXZ model with single-ion-anisotropy is the following,

$$H = \sum_{i}^{N} \left\{ \left(\hat{S}_i^x \hat{S}_{i+1}^x + \hat{S}_i^y \hat{S}_{i+1}^y + \Delta \hat{S}_i^z \hat{S}_{i+1}^z \right) + D \left(\hat{S}_i^z \right)^2 \right\} \tag{B.1.1}$$

We can identify the local term as $D \left(\hat{S}_i^z \right)^2$ and the interacting term as $\hat{S}_i^\alpha \hat{S}_{i+1}^\alpha$, $\alpha = x, y, z$. To form a block of a single site we must write these local operators in their matrix form, as appropriate, remembering that we are working with spin 1, and also write a local identity matrix for tensor products,

$$S_\alpha = \hat{S}^\alpha \qquad I = \mathcal{I} \tag{B.1.2}$$

Define the left and right block operators,

$$\begin{aligned} BlockS_\alpha L &= \hat{S}^\alpha & BlockS_\alpha R &= \hat{S}^\alpha \\ BlockIL &= \mathcal{I} & BlockIR &= \mathcal{I} \\ BlockHL &= D\hat{S}_i^{z2} & BlockHR &= D\hat{S}_i^{z2} \end{aligned} \tag{B.1.3}$$

and the site operators, for which only the local energy remains to be defined since the others were defined at the beginning

$$hL = D\hat{S}_i^{z2} \qquad hR = D\hat{S}_i^{z2} \tag{B.1.4}$$

Now for the LEB, we write it as in equation 3.2.2

$$\begin{aligned} BlockHL =& BlockHL \otimes I + BlockIL \otimes hL + \\ & (BlockS_xL \otimes S_x + BlockS_yL \otimes S_y + \Delta BlockS_zL \otimes S_z) \end{aligned} \tag{B.1.5}$$

We recall writing in the enlarged form the relevant operators,

$$\begin{aligned} BlockS_\alpha L &= BlockIL \otimes S_\alpha \\ BlockIL &= BlockIL \otimes I \end{aligned} \tag{B.1.6}$$

and likewise for the REB. Finally, following equation 3.2.4, the Hamiltonian of the superblock is

$$\begin{aligned} HS =& BlockHL \otimes BlockIR + BlockIL \otimes BlockHR + \\ & (BlockS_xL \otimes BlockS_xR + BlockS_yL \otimes BlockS_yR + \\ & J_z BlockS_zL \otimes BlockS_zR) \end{aligned} \tag{B.1.7}$$

To finish the infinite algorithm, it only remains to diagonalize the Hamiltonian of the superblock to find the ground state and construct the density matrix to finish steps 4 and 5. As mentioned before, in this work we are interested in studying the quantum correlations of the central sites of the chain, so in step 3 of the algorithm, we also trace out the degrees of freedom of the blocks to obtain the reduced density matrix of the central sites. We store this matrix in the last iteration of the algorithm for each value of (Δ, D) that we simulate.